Review | Vol. 8, No. 5 | 1 May 2017 | BIOMEDICAL OPTICS EXPRESS 2405

Biomedical Optics EXPRESS

Endoscopic optical coherence tomography: technologies and clinical applications [Invited]

MICHALINA J. GORA,[1,2] MELISSA J. SUTER,[1,3,4] GUILLERMO J. TEARNEY,[1,4,5,7] AND XINGDE LI[6,8]

[1]*Wellman Center for Photomedicine, Massachusetts General Hospital and Harvard Medical School, 55 Fruit Street, Boston, MA 02114, USA*
[2]*ICube Laboratory, CNRS, Strasbourg University, 1 Place de l'Hopital, Strasbourg 67091, France*
[3]*Department of Medicine, Division of Pulmonary and Critical Care, Massachusetts General Hospital, 55 Fruit Street, Boston, MA 02114, USA*
[4]*Harvard Medical School, 25 Shattuck Street, Boston, MA 02115, USA*
[5]*Department of Pathology, Massachusetts General Hospital, 55 Fruit Street, Boston, MA 02114, USA*
[6]*Department of Biomedical Engineering, Department of Electrical and Computer Engineering, and Department of Oncology, Johns Hopkins University, 720 Rutland Avenue, Traylor 710, Baltimore, MD 21205, USA*
[7]*gtearney@partners.org*
[8]*xingde@jhu.edu*

Abstract: In this paper, we review the current state of technology development and clinical applications of endoscopic optical coherence tomography (OCT). Key design and engineering considerations are discussed for most OCT endoscopes, including side-viewing and forward-viewing probes, along with different scanning mechanisms (proximal-scanning versus distal-scanning). Multi-modal endoscopes that integrate OCT with other imaging modalities are also discussed. The review of clinical applications of endoscopic OCT focuses heavily on diagnosis of diseases and guidance of interventions. Representative applications in several organ systems are presented, such as in the cardiovascular, digestive, respiratory, and reproductive systems. A brief outlook of the field of endoscopic OCT is also discussed.

OCIS codes: (170.4500) Optical coherence tomography; (170.2150) Endoscopic imaging; (170.1610) Clinical applications; (170.4580) Optical diagnostics for medicine.

References and links

1. T. Cao and H. L. Tey, "High-definition optical coherence tomography - an aid to clinical practice and research in dermatology," J. Dtsch. Dermatol. Ges. **13**(9), 886–890 (2015).
2. J. Olsen, L. Themstrup, and G. B. Jemec, "Optical coherence tomography in dermatology," G. Ital. Dermatol. Venereol. **150**(5), 603–615 (2015).
3. M. Ulrich, L. Themstrup, N. de Carvalho, M. Manfredi, C. Grana, S. Ciardo, R. Kästle, J. Holmes, R. Whitehead, G. B. Jemec, G. Pellacani, and J. Welzel, "Dynamic Optical Coherence Tomography in Dermatology," Dermatology (Basel) **232**(3), 298–311 (2016).
4. G. J. Tearney, S. A. Boppart, B. E. Bouma, M. E. Brezinski, N. J. Weissman, J. F. Southern, and J. G. Fujimoto, "Scanning single-mode fiber optic catheter-endoscope for optical coherence tomography," Opt. Lett. **21**(7), 543–545 (1996).
5. A. M. Rollins, R. Ung-Arunyawee, A. Chak, R. C. K. Wong, K. Kobayashi, M. V. Sivak, Jr., and J. A. Izatt, "Real-time in vivo imaging of human gastrointestinal ultrastructure by use of endoscopic optical coherence tomography with a novel efficient interferometer design," Opt. Lett. **24**(19), 1358–1360 (1999).
6. M. V. Sivak, Jr., K. Kobayashi, J. A. Izatt, A. M. Rollins, R. Ung-Runyawee, A. Chak, R. C. Wong, G. A. Isenberg, and J. Willis, "High-resolution endoscopic imaging of the GI tract using optical coherence tomography," Gastrointest. Endosc. **51**(4), 474–479 (2000).
7. J. Xi, A. Zhang, Z. Liu, W. Liang, L. Y. Lin, S. Yu, and X. Li, "Diffractive catheter for ultrahigh-resolution spectral-domain volumetric OCT imaging," Opt. Lett. **39**(7), 2016–2019 (2014).
8. P. H. Tran, D. S. Mukai, M. Brenner, and Z. Chen, "In vivo endoscopic optical coherence tomography by use of a rotational microelectromechanical system probe," Opt. Lett. **29**(11), 1236–1238 (2004).

#284474 https://doi.org/10.1364/BOE.8.002405
Journal © 2017 Received 10 Jan 2017; revised 20 Mar 2017; accepted 27 Mar 2017; published 7 Apr 2017

Biomedical Optics EXPRESS

9. P. R. Herz, Y. Chen, A. D. Aguirre, K. Schneider, P. Hsiung, J. G. Fujimoto, K. Madden, J. Schmitt, J. Goodnow, and C. Petersen, "Micromotor endoscope catheter for in vivo, ultrahigh-resolution optical coherence tomography," Opt. Lett. **29**(19), 2261–2263 (2004).
10. T.-H. Tsai, B. Potsaid, Y. K. Tao, V. Jayaraman, J. Jiang, P. J. S. Heim, M. F. Kraus, C. Zhou, J. Hornegger, H. Mashimo, A. E. Cable, and J. G. Fujimoto, "Ultrahigh speed endoscopic optical coherence tomography using micromotor imaging catheter and VCSEL technology," Biomed. Opt. Express **4**(7), 1119–1132 (2013).
11. K. Liang, G. Traverso, H.-C. Lee, O. O. Ahsen, Z. Wang, B. Potsaid, M. Giacomelli, V. Jayaraman, R. Barman, A. Cable, H. Mashimo, R. Langer, and J. G. Fujimoto, "Ultrahigh speed en face OCT capsule for endoscopic imaging," Biomed. Opt. Express **6**(4), 1146–1163 (2015).
12. T. Wang, T. Pfeiffer, E. Regar, W. Wieser, H. van Beusekom, C. T. Lancee, G. Springeling, I. Krabbendam, A. F. W. van der Steen, R. Huber, and G. van Soest, "Heartbeat OCT: in vivo intravascular megahertz-optical coherence tomography," Biomed. Opt. Express **6**(12), 5021–5032 (2015).
13. M. Strathman, Y. Liu, E. G. Keeler, M. Song, U. Baran, J. Xi, M. T. Sun, R. Wang, X. Li, and L. Y. Lin, "MEMS scanning micromirror for optical coherence tomography," Biomed. Opt. Express **6**(1), 211–224 (2015).
14. H.-C. Lee, O. O. Ahsen, K. Liang, Z. Wang, C. Cleveland, L. Booth, B. Potsaid, V. Jayaraman, A. E. Cable, H. Mashimo, R. Langer, G. Traverso, and J. G. Fujimoto, "Circumferential optical coherence tomography angiography imaging of the swine esophagus using a micromotor balloon catheter," Biomed. Opt. Express **7**(8), 2927–2942 (2016).
15. N. Uribe-Patarroyo and B. E. Bouma, "Rotational distortion correction in endoscopic optical coherence tomography based on speckle decorrelation," Opt. Lett. **40**(23), 5518–5521 (2015).
16. X. D. Li, S. A. Boppart, J. Van Dam, H. Mashimo, M. Mutinga, W. Drexler, M. Klein, C. Pitris, M. L. Krinsky, M. E. Brezinski, and J. G. Fujimoto, "Optical coherence tomography: advanced technology for the endoscopic imaging of Barrett's esophagus," Endoscopy **32**(12), 921–930 (2000).
17. B. E. Bouma and G. J. Tearney, "Power-efficient nonreciprocal interferometer and linear-scanning fiber-optic catheter for optical coherence tomography," Opt. Lett. **24**(8), 531–533 (1999).
18. V. X. Yang, M. Gordon, S. J. Tang, N. Marcon, G. Gardiner, B. Qi, S. Bisland, E. Seng-Yue, S. Lo, J. Pekar, B. Wilson, and I. Vitkin, "High speed, wide velocity dynamic range Doppler optical coherence tomography (Part III): in vivo endoscopic imaging of blood flow in the rat and human gastrointestinal tracts," Opt. Express **11**(19), 2416–2424 (2003).
19. W. Jung, J. Zhang, R. Mina-Araghi, N. Hanna, M. Brenner, J. S. Nelson, and Z. Chen, "Feasibility study of normal and septic tracheal imaging using optical coherence tomography," Lasers Surg. Med. **35**(2), 121–127 (2004).
20. X. Liu, M. J. Cobb, Y. Chen, M. B. Kimmey, and X. Li, "Rapid-scanning forward-imaging miniature endoscope for real-time optical coherence tomography," Opt. Lett. **29**(15), 1763–1765 (2004).
21. E. Zagaynova, N. Gladkova, N. Shakhova, G. Gelikonov, and V. Gelikonov, "Endoscopic OCT with forward-looking probe: clinical studies in urology and gastroenterology," J. Biophotonics **1**(2), 114–128 (2008).
22. S. Moon, S. W. Lee, M. Rubinstein, B. J. Wong, and Z. Chen, "Semi-resonant operation of a fiber-cantilever piezotube scanner for stable optical coherence tomography endoscope imaging," Opt. Express **18**(20), 21183–21197 (2010).
23. K. H. Kim, J. A. Burns, J. J. Bernstein, G. N. Maguluri, B. H. Park, and J. F. de Boer, "In vivo 3D human vocal fold imaging with polarization sensitive optical coherence tomography and a MEMS scanning catheter," Opt. Express **18**(14), 14644–14653 (2010).
24. V.-F. Duma, J. P. Rolland, and A. G. Podoleanu, "Perspectives of optical scanning in OCT," presented at BiOS, 2010.
25. C. Duan, J. Sun, S. Samuelson, and H. Xie, "Probe alignment and design issues of microelectromechanical system based optical coherence tomography endoscopic imaging," Appl. Opt. **52**(26), 6589–6598 (2013).
26. K. L. Lurie, A. A. Gurjarpadhye, E. J. Seibel, and A. K. Ellerbee, "Rapid scanning catheterscope for expanded forward-view volumetric imaging with optical coherence tomography," Opt. Lett. **40**(13), 3165–3168 (2015).
27. J. Xi, L. Huo, Y. Wu, M. J. Cobb, J. H. Hwang, and X. Li, "High-resolution OCT balloon imaging catheter with astigmatism correction," Opt. Lett. **34**(13), 1943–1945 (2009).
28. E. Swanson, C. L. Petersen, E. McNamara, R. B. Lamport, and D. L. Kelly, "Ultra-small optical probes, imaging optics, and methods for using same," U.S. Patent: 6,445,939, September 3, 2002.
29. M. S. Shishkov, G. J. Tearney, and B. E. Bouma, "Scultpured optical fiber tips for narrow diameter optical catheters," in Biomedical Topical Meeting, OSA Technical Digest. Miami Beach, Florida: Optical Society of America, 2004, pp. SE5.
30. V. X. D. Yang, Y. X. Mao, N. Munce, B. Standish, W. Kucharczyk, N. E. Marcon, B. C. Wilson, and I. A. Vitkin, "Interstitial Doppler optical coherence tomography," Opt. Lett. **30**(14), 1791–1793 (2005).
31. G. J. Tearney, M. E. Brezinski, B. E. Bouma, S. A. Boppart, C. Pitris, J. F. Southern, and J. G. Fujimoto, "In vivo endoscopic optical biopsy with optical coherence tomography," Science **276**(5321), 2037–2039 (1997).
32. J. G. Fujimoto, S. A. Boppart, G. J. Tearney, B. E. Bouma, C. Pitris, and M. E. Brezinski, "High resolution in vivo intra-arterial imaging with optical coherence tomography," Heart **82**(2), 128–133 (1999).
33. B. E. Bouma, G. J. Tearney, C. C. Compton, and N. S. Nishioka, "High-resolution imaging of the human esophagus and stomach in vivo using optical coherence tomography," Gastrointest. Endosc. **51**(4), 467–474 (2000).

Biomedical Optics EXPRESS

34. I. K. Jang, B. E. Bouma, D. H. Kang, S. J. Park, S. W. Park, K. B. Seung, K. B. Choi, M. Shishkov, K. Schlendorf, E. Pomerantsev, S. L. Houser, H. T. Aretz, and G. J. Tearney, "Visualization of coronary atherosclerotic plaques in patients using optical coherence tomography: comparison with intravascular ultrasound," J. Am. Coll. Cardiol. **39**(4), 604–609 (2002).
35. B. J. F. Wong, R. P. Jackson, S. Guo, J. M. Ridgway, U. Mahmood, J. Su, T. Y. Shibuya, R. L. Crumley, M. Gu, W. B. Armstrong, and Z. Chen, "In vivo optical coherence tomography of the human larynx: normative and benign pathology in 82 patients," Laryngoscope **115**(11), 1904–1911 (2005).
36. V. X. D. Yang, S. J. Tang, M. L. Gordon, B. Qi, G. Gardiner, M. Cirocco, P. Kortan, G. B. Haber, G. Kandel, I. A. Vitkin, B. C. Wilson, and N. E. Marcon, "Endoscopic Doppler optical coherence tomography in the human GI tract: initial experience," Gastrointest. Endosc. **61**(7), 879–890 (2005).
37. Y. Chen, A. D. Aguirre, P. L. Hsiung, S. Desai, P. R. Herz, M. Pedrosa, Q. Huang, M. Figueiredo, S. W. Huang, A. Koski, J. M. Schmitt, J. G. Fujimoto, and H. Mashimo, "Ultrahigh resolution optical coherence tomography of Barrett's esophagus: preliminary descriptive clinical study correlating images with histology," Endoscopy **39**(7), 599–605 (2007).
38. S. H. Yun, G. J. Tearney, B. J. Vakoc, M. Shishkov, W. Y. Oh, A. E. Desjardins, M. J. Suter, R. C. Chan, J. A. Evans, I.-K. Jang, N. S. Nishioka, J. F. de Boer, and B. E. Bouma, "Comprehensive volumetric optical microscopy in vivo," Nat. Med. **12**(12), 1429–1433 (2007).
39. L. P. Hariri, M. B. Applegate, M. Mino-Kenudson, E. J. Mark, B. D. Medoff, A. D. Luster, B. E. Bouma, G. J. Tearney, and M. J. Suter, "Volumetric optical frequency domain imaging of pulmonary pathology with precise correlation to histopathology," Chest **143**(1), 64–74 (2013).
40. J. Li, M. de Groot, F. Helderman, J. Mo, J. M. A. Daniels, K. Grünberg, T. G. Sutedja, and J. F. de Boer, "High speed miniature motorized endoscopic probe for optical frequency domain imaging," Opt. Express **20**(22), 24132–24138 (2012).
41. T. Wang, W. Wieser, G. Springeling, R. Beurskens, C. T. Lancee, T. Pfeiffer, A. F. W. van der Steen, R. Huber, and G. van Soest, "Intravascular optical coherence tomography imaging at 3200 frames per second," Opt. Lett. **38**(10), 1715–1717 (2013).
42. U. Oltmanns, K. Palmowski, M. Wielpütz, N. Kahn, E. Baroke, R. Eberhardt, S. Wege, M. Wiebel, M. Kreuter, F. J. Herth, and M. A. Mall, "Optical coherence tomography detects structural abnormalities of the nasal mucosa in patients with cystic fibrosis," J. Cyst. Fibros. **15**(2), 216–222 (2016).
43. T.-H. Tsai, H.-C. Lee, O. O. Ahsen, K. Liang, M. G. Giacomelli, B. M. Potsaid, Y. K. Tao, V. Jayaraman, M. Figueiredo, Q. Huang, A. E. Cable, J. Fujimoto, and H. Mashimo, "Ultrahigh speed endoscopic optical coherence tomography for gastroenterology," Biomed. Opt. Express **5**(12), 4387–4404 (2014).
44. T.-H. Tsai, O. O. Ahsen, H.-C. Lee, K. Liang, M. Figueiredo, Y. K. Tao, M. G. Giacomelli, B. M. Potsaid, V. Jayaraman, Q. Huang, A. E. Cable, J. G. Fujimoto, and H. Mashimo, "Endoscopic Optical Coherence Angiography Enables 3-Dimensional Visualization of Subsurface Microvasculature," Gastroenterology **147**(6), 1219–1221 (2014).
45. M. Pierce, M. Shishkov, B. Park, N. Nassif, B. Bouma, G. Tearney, and J. de Boer, "Effects of sample arm motion in endoscopic polarization-sensitive optical coherence tomography," Opt. Express **13**(15), 5739–5749 (2005).
46. J. Li, F. Feroldi, J. de Lange, J. M. A. Daniels, K. Grünberg, and J. F. de Boer, "Polarization sensitive optical frequency domain imaging system for endobronchial imaging," Opt. Express **23**(3), 3390–3402 (2015).
47. A. R. Tumlinson, J. K. Barton, B. Považay, H. Sattman, A. Unterhuber, R. A. Leitgeb, and W. Drexler, "Endoscope-tip interferometer for ultrahigh resolution frequency domain optical coherence tomography in mouse colon," Opt. Express **14**(5), 1878–1887 (2006).
48. U. Sharma and J. U. Kang, "Common-path optical coherence tomography with side-viewing bare fiber probe for endoscopic optical coherence tomography," Rev. Sci. Instrum. **78**(11), 113102 (2007).
49. Y. Pan, H. Xie, and G. K. Fedder, "Endoscopic optical coherence tomography based on a microelectromechanical mirror," Opt. Lett. **26**(24), 1966–1968 (2001).
50. W. Jung, D. T. McCormick, J. Zhang, L. Wang, N. C. Tien, and Z. Chen, "Three-dimensional endoscopic optical coherence tomography by use of a two-axis microelectromechanical scanning mirror," Appl. Phys. Lett. **88**(16), 163901 (2006).
51. M. Strathman, Y. Liu, X. Li, and L. Y. Lin, "Dynamic focus-tracking MEMS scanning micromirror with low actuation voltages for endoscopic imaging," Opt. Express **21**(20), 23934–23941 (2013).
52. J. Sun, S. Guo, L. Wu, L. Liu, S.-W. Choe, B. S. Sorg, and H. Xie, "3D in vivo optical coherence tomography based on a low-voltage, large-scan-range 2D MEMS mirror," Opt. Express **18**(12), 12065–12075 (2010).
53. X. Zhang, C. Duan, L. Liu, X. Li, and H. Xie, "A non-resonant fiber scanner based on an electrothermally-actuated MEMS stage," Sens. Actuators A Phys. **233**, 239–245 (2015).
54. Y.-H. Seo, K. Hwang, H.-C. Park, and K.-H. Jeong, "Electrothermal MEMS fiber scanner for optical endomicroscopy," Opt. Express **24**(4), 3903–3909 (2016).
55. A. Sergeev, V. Gelikonov, G. Gelikonov, F. Feldchtein, R. Kuranov, N. Gladkova, N. Shakhova, L. Snopova, A. Shakhov, I. Kuznetzova, A. Denisenko, V. Pochinko, Y. Chumakov, and O. Streltzova, "In vivo endoscopic OCT imaging of precancer and cancer states of human mucosa," Opt. Express **1**(13), 432–440 (1997).
56. V. M. Gelikonov, G. V. Gelikonov, N. D. Gladkova, N. M. Shahova, F. I. Feldchtein, and A. M. Sergeev, "Optical coherent tomography apparatus, fiberoptic lateral scanner and method for studying biological tissues in vivo," U.S. Patent: 6,608,684, August 19, 2003.

Biomedical Optics EXPRESS

57. M. J. Cobb, X. Liu, and X. Li, "Continuous focus tracking for real-time optical coherence tomography," Opt. Lett. **30**(13), 1680–1682 (2005).
58. E. J. Seibel and Q. Y. J. Smithwick, "Unique features of optical scanning, single fiber endoscopy," Lasers Surg. Med. **30**(3), 177–183 (2002).
59. L. Huo, J. Xi, Y. Wu, and X. Li, "Forward-viewing resonant fiber-optic scanning endoscope of appropriate scanning speed for 3D OCT imaging," Opt. Express **18**(14), 14375–14384 (2010).
60. W. Liang, K. Murari, Y. Zhang, Y. Chen, M. J. Li, and X. Li, "Increased illumination uniformity and reduced photodamage offered by the Lissajous scanning in fiber-optic two-photon endomicroscopy," J. Biomed. Opt. **17**(2), 021108 (2012).
61. N. Zhang, T.-H. Tsai, O. O. Ahsen, K. Liang, H.-C. Lee, P. Xue, X. Li, and J. G. Fujimoto, "Compact piezoelectric transducer fiber scanning probe for optical coherence tomography," Opt. Lett. **39**(2), 186–188 (2014).
62. J. Wu, M. Conry, C. Gu, F. Wang, Z. Yaqoob, and C. Yang, "Paired-angle-rotation scanning optical coherence tomography forward-imaging probe," Opt. Lett. **31**(9), 1265–1267 (2006).
63. T. Xie, D. Mukai, S. Guo, M. Brenner, and Z. Chen, "Fiber-optic-bundle-based optical coherence tomography," Opt. Lett. **30**(14), 1803–1805 (2005).
64. H. D. Ford and R. P. Tatam, "Characterization of optical fiber imaging bundles for swept-source optical coherence tomography," Appl. Opt. **50**(5), 627–640 (2011).
65. J.-H. Han and J. U. Kang, "Effect of multimodal coupling in imaging micro-endoscopic fiber bundle on optical coherence tomography," Appl. Phys. B **106**(3), 635–643 (2012).
66. M. D. Risi, H. Makhlouf, A. R. Rouse, and A. F. Gmitro, "Analysis of multimode fiber bundles for endoscopic spectral-domain optical coherence tomography," Appl. Opt. **54**(1), 101–113 (2015).
67. J. W. Pyhtila, J. D. Boyer, K. J. Chalut, and A. Wax, "Fourier-domain angle-resolved low coherence interferometry through an endoscopic fiber bundle for light-scattering spectroscopy," Opt. Lett. **31**(6), 772–774 (2006).
68. Y. Zhu, N. G. Terry, J. T. Woosley, N. J. Shaheen, and A. Wax, "Design and validation of an angle-resolved low-coherence interferometry fiber probe for in vivo clinical measurements of depth-resolved nuclear morphology," J. Biomed. Opt. **16**(1), 011003 (2011).
69. D. C. Adler, Y. Chen, R. Huber, J. Schmitt, J. Connolly, and J. G. Fujimoto, "Three-dimensional endomicroscopy using optical coherence tomography," Nat. Photonics **1**(12), 709–716 (2007).
70. J. M. Tobis, J. Mallery, D. Mahon, K. Lehmann, P. Zalesky, J. Griffith, J. Gessert, M. Moriuchi, M. McRae, and M. L. Dwyer, "Intravascular ultrasound imaging of human coronary arteries in vivo. Analysis of tissue characterizations with comparison to in vitro histological specimens," Circulation **83**(3), 913–926 (1991).
71. T.-H. Tsai, B. Potsaid, M. F. Kraus, C. Zhou, Y. K. Tao, J. Hornegger, and J. G. Fujimoto, "Piezoelectric-transducer-based miniature catheter for ultrahigh-speed endoscopic optical coherence tomography," Biomed. Opt. Express **2**(8), 2438–2448 (2011).
72. B. J. Vakoc, M. Shishko, S. H. Yun, W.-Y. Oh, M. J. Suter, A. E. Desjardins, J. A. Evans, N. S. Nishioka, G. J. Tearney, and B. E. Bouma, "Comprehensive esophageal microscopy by using optical frequency-domain imaging (with video)," Gastrointest. Endosc. **65**(6), 898–905 (2007).
73. H. L. Fu, Y. Leng, M. J. Cobb, K. Hsu, J. H. Hwang, and X. Li, "Flexible miniature compound lens design for high-resolution optical coherence tomography balloon imaging catheter," J. Biomed. Opt. **13**(6), 060502 (2008).
74. W. Kang, H. Wang, Y. Pan, M. W. Jenkins, G. A. Isenberg, A. Chak, M. Atkinson, D. Agrawal, Z. Hu, and A. M. Rollins, "Endoscopically guided spectral-domain OCT with double-balloon catheters," Opt. Express **18**(16), 17364–17372 (2010).
75. M. J. Gora, J. S. Sauk, R. W. Carruth, K. A. Gallagher, M. J. Suter, N. S. Nishioka, L. E. Kava, M. Rosenberg, B. E. Bouma, and G. J. Tearney, "Tethered capsule endomicroscopy enables less invasive imaging of gastrointestinal tract microstructure," Nat. Med. **19**(2), 238–240 (2013).
76. X. Li, C. Chudoba, T. Ko, C. Pitris, and J. G. Fujimoto, "Imaging needle for optical coherence tomography," Opt. Lett. **25**(20), 1520–1522 (2000).
77. X. Li, T. H. Ko, and J. G. Fujimoto, "Intraluminal fiber-optic Doppler imaging catheter for structural and functional optical coherence tomography," Opt. Lett. **26**(23), 1906–1908 (2001).
78. Y. C. Wu, J. F. Xi, L. Huo, J. Padvorac, E. Shin, S. A. Giday, A. A. Lennon, M. I. F. Canto, J. H. Hwang, and X. D. Li, "Robust high-resolution fine OCT needle for side-viewing interstitial tissue imaging," IEEE J. Sel. Top. Quantum Electron. **16**(4), 863–869 (2010).
79. D. Lorenser, X. Yang, R. W. Kirk, B. C. Quirk, R. A. McLaughlin, and D. D. Sampson, "Ultrathin side-viewing needle probe for optical coherence tomography," Opt. Lett. **36**(19), 3894–3896 (2011).
80. C.-P. Liang, J. Wierwille, T. Moreira, G. Schwartzbauer, M. S. Jafri, C.-M. Tang, and Y. Chen, "A forward-imaging needle-type OCT probe for image guided stereotactic procedures," Opt. Express **19**(27), 26283–26294 (2011).
81. M. Villiger, D. Lorenser, R. A. McLaughlin, B. C. Quirk, R. W. Kirk, B. E. Bouma, and D. D. Sampson, "Deep tissue volume imaging of birefringence through fibre-optic needle probes for the delineation of breast tumour," Sci. Rep. **6**(1), 28771 (2016).
82. K. M. Tan, M. Shishkov, A. Chee, M. B. Applegate, B. E. Bouma, and M. J. Suter, "Flexible transbronchial optical frequency domain imaging smart needle for biopsy guidance," Biomed. Opt. Express **3**(8), 1947–1954 (2012).

Biomedical Optics EXPRESS

83. L. Scolaro, D. Lorenser, R. A. McLaughlin, B. C. Quirk, R. W. Kirk, and D. D. Sampson, "High-sensitivity anastigmatic imaging needle for optical coherence tomography," Opt. Lett. **37**(24), 5247–5249 (2012).
84. A. R. Tumlinson, B. Povazay, L. P. Hariri, J. McNally, A. Unterhuber, B. Hermann, H. Sattmann, W. Drexler, and J. K. Barton, "In vivo ultrahigh-resolution optical coherence tomography of mouse colon with an achromatized endoscope," J. Biomed. Opt. **11**(6), 064003 (2006).
85. D. Wang, B. V. Hunter, M. J. Cobb, and X. D. Li, "Super-achromatic rapid scanning microendoscope for ultrahigh-resolution OCT imaging," IEEE J. Sel. Top. Quantum Electron. **13**(6), 1596–1601 (2007).
86. W. Yuan, J. Mavadia-Shukla, J. Xi, W. Liang, X. Yu, S. Yu, and X. Li, "Optimal operational conditions for supercontinuum-based ultrahigh-resolution endoscopic OCT imaging," Opt. Lett. **41**(2), 250–253 (2016).
87. J. Mavadia, J. Xi, Y. Chen, and X. Li, "An all-fiber-optic endoscopy platform for simultaneous OCT and fluorescence imaging," Biomed. Opt. Express **3**(11), 2851–2859 (2012).
88. A. R. Tumlinson, L. P. Hariri, U. Utzinger, and J. K. Barton, "Miniature endoscope for simultaneous optical coherence tomography and laser-induced fluorescence measurement," Appl. Opt. **43**(1), 113–121 (2004).
89. S. Y. Ryu, H. Y. Choi, J. Na, E. S. Choi, and B. H. Lee, "Combined system of optical coherence tomography and fluorescence spectroscopy based on double-cladding fiber," Opt. Lett. **33**(20), 2347–2349 (2008).
90. H. Yoo, J. W. Kim, M. Shishkov, E. Namati, T. Morse, R. Shubochkin, J. R. McCarthy, V. Ntziachristos, B. E. Bouma, F. A. Jaffer, and G. J. Tearney, "Intra-arterial catheter for simultaneous microstructural and molecular imaging in vivo," Nat. Med. **17**(12), 1680–1684 (2011).
91. S. Liang, A. Saidi, J. Jing, G. Liu, J. Li, J. Zhang, C. Sun, J. Narula, and Z. Chen, "Intravascular atherosclerotic imaging with combined fluorescence and optical coherence tomography probe based on a double-clad fiber combiner," J. Biomed. Opt. **17**(7), 0705011 (2012).
92. D. Lorenser, B. C. Quirk, M. Auger, W.-J. Madore, R. W. Kirk, N. Godbout, D. D. Sampson, C. Boudoux, and R. A. McLaughlin, "Dual-modality needle probe for combined fluorescence imaging and three-dimensional optical coherence tomography," Opt. Lett. **38**(3), 266–268 (2013).
93. L. Scolaro, D. Lorenser, W.-J. Madore, R. W. Kirk, A. S. Kramer, G. C. Yeoh, N. Godbout, D. D. Sampson, C. Boudoux, and R. A. McLaughlin, "Molecular imaging needles: dual-modality optical coherence tomography and fluorescence imaging of labeled antibodies deep in tissue," Biomed. Opt. Express **6**(5), 1767–1781 (2015).
94. S. Feng, F.-A. Zeng, and B. Chance, "Photon migration in the presence of a single defect: a perturbation analysis," Appl. Opt. **34**(19), 3826–3837 (1995).
95. M. S. Patterson, S. Andersson-Engels, B. C. Wilson, and E. K. Osei, "Absorption spectroscopy in tissue-simulating materials: a theoretical and experimental study of photon paths," Appl. Opt. **34**(1), 22–30 (1995).
96. T. Durduran, R. Choe, W. B. Baker, and A. G. Yodh, "Diffuse optics for tissue monitoring and tomography," Reports on progress in physics. Physical Society (Great Britain) **73**(7), 076701 (2010).
97. A. M. Fard, P. Vacas-Jacques, E. Hamidi, H. Wang, R. W. Carruth, J. A. Gardecki, and G. J. Tearney, "Optical coherence tomography--near infrared spectroscopy system and catheter for intravascular imaging," Opt. Express **21**(25), 30849–30858 (2013).
98. J. Xi, Y. Chen, Y. Zhang, K. Murari, M.-J. Li, and X. Li, "Integrated multimodal endomicroscopy platform for simultaneous en face optical coherence and two-photon fluorescence imaging," Opt. Lett. **37**(3), 362–364 (2012).
99. X. Li, J. Yin, C. Hu, Q. Zhou, K. K. Shung, and Z. Chen, "High-resolution coregistered intravascular imaging with integrated ultrasound and optical coherence tomography probe," Appl. Phys. Lett. **97**(13), 133702 (2010).
100. J. Yin, H.-C. Yang, X. Li, J. Zhang, Q. Zhou, C. Hu, K. K. Shung, and Z. Chen, "Integrated intravascular optical coherence tomography ultrasound imaging system," J. Biomed. Opt. **15**(1), 010512 (2010).
101. J. Yin, X. Li, J. Jing, J. Li, D. Mukai, S. Mahon, A. Edris, K. Hoang, K. K. Shung, M. Brenner, J. Narula, Q. Zhou, and Z. Chen, "Novel combined miniature optical coherence tomography ultrasound probe for in vivo intravascular imaging," J. Biomed. Opt. **16**(6), 060505 (2011).
102. Y. Yang, X. Li, T. Wang, P. D. Kumavor, A. Aguirre, K. K. Shung, Q. Zhou, M. Sanders, M. Brewer, and Q. Zhu, "Integrated optical coherence tomography, ultrasound and photoacoustic imaging for ovarian tissue characterization," Biomed. Opt. Express **2**(9), 2551–2561 (2011).
103. X. Dai, L. Xi, C. Duan, H. Yang, H. Xie, and H. Jiang, "Miniature probe integrating optical-resolution photoacoustic microscopy, optical coherence tomography, and ultrasound imaging: proof-of-concept," Opt. Lett. **40**(12), 2921–2924 (2015).
104. H. Yabushita, B. E. Bouma, S. L. Houser, H. T. Aretz, I. K. Jang, K. H. Schlendorf, C. R. Kauffman, M. Shishkov, D. H. Kang, E. F. Halpern, and G. J. Tearney, "Characterization of human atherosclerosis by optical coherence tomography," Circulation **106**(13), 1640–1645 (2002).
105. S. Nishimura, S. Ehara, T. Hasegawa, K. Matsumoto, J. Yoshikawa, and K. Shimada, "Cholesterol crystal as a new feature of coronary vulnerable plaques: An optical coherence tomography study," J. Cardiol. **69**(1), 253–259 (2017).
106. T. Kume, T. Akasaka, T. Kawamoto, Y. Ogasawara, N. Watanabe, E. Toyota, Y. Neishi, R. Sukmawan, Y. Sadahira, and K. Yoshida, "Assessment of coronary arterial thrombus by optical coherence tomography," Am. J. Cardiol. **97**(12), 1713–1717 (2006).
107. B. D. MacNeill, I. K. Jang, B. E. Bouma, N. Iftimia, M. Takano, H. Yabushita, M. Shishkov, C. R. Kauffman, S. L. Houser, H. T. Aretz, D. DeJoseph, E. F. Halpern, and G. J. Tearney, "Focal and multi-focal plaque macrophage distributions in patients with acute and stable presentations of coronary artery disease," J. Am. Coll. Cardiol. **44**(5), 972–979 (2004).

Biomedical Optics EXPRESS

108. L. Di Vito, M. Agozzino, V. Marco, A. Ricciardi, M. Concardi, E. Romagnoli, L. Gatto, G. Calogero, L. Tavazzi, E. Arbustini, and F. Prati, "Identification and quantification of macrophage presence in coronary atherosclerotic plaques by optical coherence tomography," Eur. Heart J. Cardiovasc. Imaging **16**(7), 807–813 (2015).
109. G. J. Tearney, E. Regar, T. Akasaka, T. Adriaenssens, P. Barlis, H. G. Bezerra, B. Bouma, N. Bruining, J. M. Cho, S. Chowdhary, M. A. Costa, R. de Silva, J. Dijkstra, C. Di Mario, D. Dudek, E. Falk, M. D. Feldman, P. Fitzgerald, H. M. Garcia-Garcia, N. Gonzalo, J. F. Granada, G. Guagliumi, N. R. Holm, Y. Honda, F. Ikeno, M. Kawasaki, J. Kochman, L. Koltowski, T. Kubo, T. Kume, H. Kyono, C. C. Lam, G. Lamouche, D. P. Lee, M. B. Leon, A. Maehara, O. Manfrini, G. S. Mintz, K. Mizuno, M. A. Morel, S. Nadkarni, H. Okura, H. Otake, A. Pietrasik, F. Prati, L. Räber, M. D. Radu, J. Rieber, M. Riga, A. Rollins, M. Rosenberg, V. Sirbu, P. W. Serruys, K. Shimada, T. Shinke, J. Shite, E. Siegel, S. Sonoda, M. Suter, S. Takarada, A. Tanaka, M. Terashima, T. Thim, S. Uemura, G. J. Ughi, H. M. van Beusekom, A. F. van der Steen, G. A. van Es, G. van Soest, R. Virmani, S. Waxman, N. J. Weissman, and G. Weisz, "Consensus standards for acquisition, measurement, and reporting of intravascular optical coherence tomography studies: a report from the International Working Group for Intravascular Optical Coherence Tomography Standardization and Validation," J. Am. Coll. Cardiol. **59**(12), 1058–1072 (2012).
110. R. Vergallo, T. Yonetsu, K. Kato, H. Jia, F. Abtahian, J. Tian, S. Hu, I. McNulty, B. Yu, L. M. Biasucci, F. Crea, and I.-K. Jang, "Evaluation of culprit lesions by optical coherence tomography in patients with ST-elevation myocardial infarction," Int. J. Cardiol. **168**(2), 1592–1593 (2013).
111. G. J. Ughi, H. Wang, E. Gerbaud, J. A. Gardecki, A. M. Fard, E. Hamidi, P. Vacas-Jacques, M. Rosenberg, F. A. Jaffer, and G. J. Tearney, "Clinical characterization of coronary atherosclerosis with dual-modality OCT and near-infrared autofluorescence imaging," JACC Cardiovasc. Imaging **9**(11), 1304–1314 (2016).
112. K. A. Birkmeier, A. Kastrati, R. A. Byrne, H. Holle, S. Schulz, K. Tiroch, S. Kufner, S. Massberg, K. L. Laugwitz, A. Schömig, and J. Mehilli, "Five-year clinical outcomes of sirolimus-eluting versus paclitaxel-eluting stents in high-risk patients," Catheter. Cardiovasc. Interv. **77**(4), 494–501 (2011).
113. J. M. Stolker, D. J. Cohen, K. F. Kennedy, M. J. Pencina, J. B. Lindsey, L. Mauri, D. E. Cutlip, and N. S. Kleima; Evaluation of Drug-Eluting Stents and Ischemic Events (EVENT) Investigators, "Repeat revascularization after contemporary percutaneous coronary intervention: an evaluation of staged, target lesion, and other unplanned revascularization procedures during the first year," Circ. Cardiovasc. Interv. **5**(6), 772–782 (2012).
114. F. Prati, L. Di Vito, G. Biondi-Zoccai, M. Occhipinti, A. La Manna, C. Tamburino, F. Burzotta, C. Trani, I. Porto, V. Ramazzotti, F. Imola, A. Manzoli, L. Materia, A. Cremonesi, and M. Albertucci, "Angiography alone versus angiography plus optical coherence tomography to guide decision-making during percutaneous coronary intervention: the Centro per la Lotta contro l'Infarto-Optimisation of Percutaneous Coronary Intervention (CLI-OPCI) study," EuroIntervention **8**(7), 823–829 (2012).
115. W. Wijns, J. Shite, M. R. Jones, S. W. Lee, M. J. Price, F. Fabbiocchi, E. Barbato, T. Akasaka, H. Bezerra, and D. Holmes, "Optical coherence tomography imaging during percutaneous coronary intervention impacts physician decision-making: ILUMIEN I study," Eur. Heart J. **36**(47), 3346–3355 (2015).
116. T. Higuma, T. Soeda, N. Abe, M. Yamada, H. Yokoyama, S. Shibutani, R. Vergallo, Y. Minami, D. S. Ong, H. Lee, K. Okumura, and I. K. Jang, "A combined optical coherence tomography and intravascular ultrasound study on plaque rupture, plaque erosion, and calcified nodule in patients with ST-segment elevation myocardial infarction: incidence, morphologic characteristics, and outcomes after percutaneous coronary intervention," JACC Cardiovasc. Interv. **8**(9), 1166–1176 (2015).
117. Z. A. Ali, A. Maehara, P. Généreux, R. A. Shlofmitz, F. Fabbiocchi, T. M. Nazif, G. Guagliumi, P. M. Meraj, F. Alfonso, H. Samady, T. Akasaka, E. B. Carlson, M. A. Leesar, M. Matsumura, M. O. Ozan, G. S. Mintz, O. Ben-Yehuda, and G. W. Stone; ILUMIEN III: OPTIMIZE PCI Investigators, "Optical coherence tomography compared with intravascular ultrasound and with angiography to guide coronary stent implantation (ILUMIEN III: OPTIMIZE PCI): a randomised controlled trial," Lancet **388**(10060), 2618–2628 (2016).
118. E. A. Mehanna, G. F. Attizzani, H. Kyono, M. Hake, and H. G. Bezerra, "Assessment of coronary stent by optical coherence tomography, methodology and definitions," Int. J. Cardiovasc. Imaging **27**(2), 259–269 (2011).
119. M. R. Selmon, A. G. Schwindt, I. M. Cawich, J. R. Chamberlin, T. S. Das, T. P. Davis, J. C. George, S. F. Janzer, L. A. Lopez, H. B. McDaniel, J. F. McKinsey, J. P. Pigott, M. L. Raja, B. Reimers, and T. L. Schreiber, "Final results of the chronic total occlusion crossing with the Ocelot System II (CONNECT II) study," J. Endovasc. Ther. **20**(6), 770–781 (2013).
120. R. F. Souza and S. J. Spechler, "Concepts in the prevention of adenocarcinoma of the distal esophagus and proximal stomach," CA Cancer J. Clin. **55**(6), 334–351 (2005).
121. J. M. Poneros, S. Brand, B. E. Bouma, G. J. Tearney, C. C. Compton, and N. S. Nishioka, "Diagnosis of specialized intestinal metaplasia by optical coherence tomography," Gastroenterology **120**(1), 7–12 (2001).
122. V. X. Yang, M. Gordon, S. J. Tang, N. Marcon, G. Gardiner, B. Qi, S. Bisland, E. Seng-Yue, S. Lo, J. Pekar, B. Wilson, and I. Vitkin, "High speed, wide velocity dynamic range Doppler optical coherence tomography (Part III): in vivo endoscopic imaging of blood flow in the rat and human gastrointestinal tracts," Opt. Express **11**(19), 2416–2424 (2003).
123. J. M. Poneros and N. S. Nishioka, "Diagnosis of Barrett's esophagus using optical coherence tomography," Gastrointest. Endosc. Clin. N. Am. **13**(2), 309–323 (2003).

Biomedical Optics EXPRESS

124. J. A. Evans and N. S. Nishioka, "The use of optical coherence tomography in screening and surveillance of Barrett's esophagus," Clin. Gastroenterol. Hepatol. **3**(7), S8–S11 (2005).
125. R. C. Haggitt, "Barrett's esophagus, dysplasia, and adenocarcinoma," Hum. Pathol. **25**(10), 982–993 (1994).
126. E. Montgomery, M. P. Bronner, J. R. Goldblum, J. K. Greenson, M. M. Haber, J. Hart, L. W. Lamps, G. Y. Lauwers, A. J. Lazenby, D. N. Lewin, M. E. Robert, A. Y. Toledano, Y. Shyr, and K. Washington, "Reproducibility of the diagnosis of dysplasia in Barrett esophagus: a reaffirmation," Hum. Pathol. **32**(4), 368–378 (2001).
127. G. Isenberg, M. V. Sivak, Jr., A. Chak, R. C. Wong, J. E. Willis, B. Wolf, D. Y. Rowland, A. Das, and A. Rollins, "Accuracy of endoscopic optical coherence tomography in the detection of dysplasia in Barrett's esophagus: a prospective, double-blinded study," Gastrointest. Endosc. **62**(6), 825–831 (2005).
128. J. A. Evans, J. M. Poneros, B. E. Bouma, J. Bressner, E. F. Halpern, M. Shishkov, G. Y. Lauwers, M. Mino-Kenudson, N. S. Nishioka, and G. J. Tearney, "Optical coherence tomography to identify intramucosal carcinoma and high-grade dysplasia in Barrett's esophagus," Clin. Gastroenterol. Hepatol. **4**(1), 38–43 (2006).
129. M. J. Suter, B. J. Vakoc, P. S. Yachimski, M. Shishkov, G. Y. Lauwers, M. Mino-Kenudson, B. E. Bouma, N. S. Nishioka, and G. J. Tearney, "Comprehensive microscopy of the esophagus in human patients with optical frequency domain imaging," Gastrointest. Endosc. **68**(4), 745–753 (2008).
130. D. C. Adler, C. Zhou, T.-H. Tsai, H.-C. Lee, L. Becker, J. M. Schmitt, Q. Huang, J. G. Fujimoto, and H. Mashimo, "Three-dimensional optical coherence tomography of Barrett's esophagus and buried glands beneath neosquamous epithelium following radiofrequency ablation," Endoscopy **41**(9), 773–776 (2009).
131. H. C. Wolfsen, P. Sharma, M. B. Wallace, C. Leggett, G. Tearney, and K. K. Wang, "Safety and feasibility of volumetric laser endomicroscopy in patients with Barrett's esophagus (with videos)," Gastrointest. Endosc. **82**(4), 631–640 (2015).
132. M. J. Suter, P. A. Jillella, B. J. Vakoc, E. F. Halpern, M. Mino-Kenudson, G. Y. Lauwers, B. E. Bouma, N. S. Nishioka, and G. J. Tearney, "Image-guided biopsy in the esophagus through comprehensive optical frequency domain imaging and laser marking: a study in living swine," Gastrointest. Endosc. **71**(2), 346–353 (2010).
133. M. J. Suter, M. J. Gora, G. Y. Lauwers, T. Arnason, J. Sauk, K. A. Gallagher, L. Kava, K. M. Tan, A. R. Soomro, T. P. Gallagher, J. A. Gardecki, B. E. Bouma, M. Rosenberg, N. S. Nishioka, and G. J. Tearney, "Esophageal-guided biopsy with volumetric laser endomicroscopy and laser cautery marking: a pilot clinical study," Gastrointest. Endosc. **79**(6), 886–896 (2014).
134. R. Huber, M. Wojtkowski, and J. G. Fujimoto, "Fourier Domain Mode Locking (FDML): A new laser operating regime and applications for optical coherence tomography," Opt. Express **14**(8), 3225–3237 (2006).
135. O. O. Ahsen, Y. K. Tao, B. M. Potsaid, Y. Sheikine, J. Jiang, I. Grulkowski, T.-H. Tsai, V. Jayaraman, M. F. Kraus, J. L. Connolly, J. Hornegger, A. Cable, and J. G. Fujimoto, "Swept source optical coherence microscopy using a 1310 nm VCSEL light source," Opt. Express **21**(15), 18021–18033 (2013).
136. T.-H. Tsai, C. Zhou, Y. K. Tao, H.-C. Lee, O. O. Ahsen, M. Figueiredo, T. Kirtane, D. C. Adler, J. M. Schmitt, Q. Huang, J. G. Fujimoto, and H. Mashimo, "Structural markers observed with endoscopic 3-dimensional optical coherence tomography correlating with Barrett's esophagus radiofrequency ablation treatment response (with videos)," Gastrointest. Endosc. **76**(6), 1104–1112 (2012).
137. K. Liang, O. O. Ahsen, H. C. Lee, Z. Wang, B. M. Potsaid, M. Figueiredo, V. Jayaraman, A. E. Cable, Q. Huang, H. Mashimo, and J. G. Fujimoto, "Volumetric mapping of Barrett's esophagus and dysplasia with en face optical coherence tomography tethered capsule," Am. J. Gastroenterol. **111**(11), 1664–1666 (2016).
138. H.-C. Lee, O. O. Ahsen, K. Liang, Z. Wang, M. Figueiredo, M. G. Giacomelli, B. Potsaid, Q. Huang, H. Mashimo, and J. G. Fujimoto, "Endoscopic optical coherence tomography angiography microvascular features associated with dysplasia in Barrett's esophagus: a pilot study (with video)," Gastrointest. Endosc. in press.
139. M. J. Gora, J. S. Sauk, R. W. Carruth, W. Lu, D. T. Carlton, A. Soomro, M. Rosenberg, N. S. Nishioka, and G. J. Tearney, "Imaging the upper gastrointestinal tract in unsedated patients using tethered capsule endomicroscopy," Gastroenterology **145**(4), 723–725 (2013).
140. M. J. Gora, L. H. Simmons, L. Quénéhervé, C. N. Grant, R. W. Carruth, W. Lu, A. Tiernan, J. Dong, B. Walker-Corkery, A. Soomro, M. Rosenberg, J. P. Metlay, and G. J. Tearney, "Tethered capsule endomicroscopy: from bench to bedside at a primary care practice," J. Biomed. Opt. **21**(10), 104001 (2016).
141. S. Jäckle, N. Gladkova, F. Feldchtein, A. Terentieva, B. Brand, G. Gelikonov, V. Gelikonov, A. Sergeev, A. Fritscher-Ravens, J. Freund, U. Seitz, S. Schröder, and N. Soehendra, "In vivo endoscopic optical coherence tomography of esophagitis, Barrett's esophagus, and adenocarcinoma of the esophagus," Endoscopy **32**(10), 750–755 (2000).
142. W. Hatta, K. Uno, T. Koike, S. Yokosawa, K. Iijima, A. Imatani, and T. Shimosegawa, "Optical coherence tomography for the staging of tumor infiltration in superficial esophageal squamous cell carcinoma," Gastrointest. Endosc. **71**(6), 899–906 (2010).
143. W. Hatta, K. Uno, T. Koike, K. Iijima, N. Asano, A. Imatani, and T. Shimosegawa, "A prospective comparative study of optical coherence tomography and EUS for tumor staging of superficial esophageal squamous cell carcinoma," Gastrointest. Endosc. **76**(3), 548–555 (2012).
144. G. Zuccaro, N. Gladkova, J. Vargo, F. Feldchtein, E. Zagaynova, D. Conwell, G. Falk, J. Goldblum, J. Dumot, J. Ponsky, G. Gelikonov, B. Davros, E. Donchenko, and J. Richter, "Optical coherence tomography of the esophagus and proximal stomach in health and disease," Am. J. Gastroenterol. **96**(9), 2633–2639 (2001).
145. G. Isenberg and M. V. Sivak, Jr., "Gastrointestinal optical coherence tomography," Tech. Gastrointest. Endosc. **5**(2), 94–101 (2003).

Biomedical Optics EXPRESS

146. A. D. Hopper, S. S. Cross, and D. S. Sanders, "Patchy villous atrophy in adult patients with suspected gluten-sensitive enteropathy: is a multiple duodenal biopsy strategy appropriate?" Endoscopy **40**(3), 219–224 (2008).
147. E. Masci, B. Mangiavillano, G. Barera, B. Parma, L. Albarello, A. Mariani, C. Doglioni, and P. A. Testoni, "Optical coherence tomography in pediatric patients: a feasible technique for diagnosing celiac disease in children with villous atrophy," Dig. Liver Dis. **41**(9), 639–643 (2009).
148. A. Das, M. V. Sivak, Jr., A. Chak, R. C. Wong, V. Westphal, A. M. Rollins, J. Willis, G. Isenberg, and J. A. Izatt, "High-resolution endoscopic imaging of the GI tract: a comparative study of optical coherence tomography versus high-frequency catheter probe EUS," Gastrointest. Endosc. **54**(2), 219–224 (2001).
149. P. Pfau, M. V. Slvak, A. Chak, M. Kinnard, G. A. Isenberg, I. J.A. A. Rollins, and V. Westphal, "Criteria for the diagnosis of dysplasie by endoscopic optical coherence tomography," Gastrointest. Endosc. **58**, 196–202 (2003).
150. B. Shen, G. Zuccaro, Jr., T. L. Gramlich, N. Gladkova, P. Trolli, M. Kareta, C. P. Delaney, J. T. Connor, B. A. Lashner, C. L. Bevins, F. Feldchtein, F. H. Remzi, M. L. Bambrick, and V. W. Fazio, "In vivo colonoscopic optical coherence tomography for transmural inflammation in inflammatory bowel disease," Clin. Gastroenterol. Hepatol. **2**(12), 1080–1087 (2004).
151. P. Consolo, G. Strangio, C. Luigiano, G. Giacobbe, S. Pallio, and L. Familiari, "Optical coherence tomography in inflammatory bowel disease: prospective evaluation of 35 patients," Dis. Colon Rectum **51**(9), 1374–1380 (2008).
152. D. C. Adler, C. Zhou, T.-H. Tsai, J. Schmitt, Q. Huang, H. Mashimo, and J. G. Fujimoto, "Three-dimensional endomicroscopy of the human colon using optical coherence tomography," Opt. Express **17**(2), 784–796 (2009).
153. P. V. Draganov, S. Chauhan, M. S. Wagh, A. R. Gupte, T. Lin, W. Hou, and C. E. Forsmark, "Diagnostic accuracy of conventional and cholangioscopy-guided sampling of indeterminate biliary lesions at the time of ERCP: a prospective, long-term follow-up study," Gastrointest. Endosc. **75**(2), 347–353 (2012).
154. M. Arvanitakis, L. Hookey, G. Tessier, P. Demetter, N. Nagy, A. Stellke, V. De Maertelaer, J. Devière, and O. Le Moine, "Intraductal optical coherence tomography during endoscopic retrograde cholangiopancreatography for investigation of biliary strictures," Endoscopy **41**(8), 696–701 (2009).
155. U. Seitz, J. Freund, S. Jaeckle, F. Feldchtein, S. Bohnacker, F. Thonke, N. Gladkova, B. Brand, S. Schröder, and N. Soehendra, "First in vivo optical coherence tomography in the human bile duct," Endoscopy **33**(12), 1018–1021 (2001).
156. J. M. Poneros, G. J. Tearney, M. Shiskov, P. B. Kelsey, G. Y. Lauwers, N. S. Nishioka, and B. E. Bouma, "Optical coherence tomography of the biliary tree during ERCP," Gastrointest. Endosc. **55**(1), 84–88 (2002).
157. P. A. Testoni, A. Mariani, B. Mangiavillano, P. G. Arcidiacono, S. Di Pietro, and E. Masci, "Intraductal optical coherence tomography for investigating main pancreatic duct strictures," Am. J. Gastroenterol. **102**(2), 269–274 (2007).
158. S. Lam, B. Standish, C. Baldwin, A. McWilliams, J. leRiche, A. Gazdar, A. I. Vitkin, V. Yang, N. Ikeda, and C. MacAulay, "In vivo optical coherence tomography imaging of preinvasive bronchial lesions," Clin. Cancer Res. **14**(7), 2006–2011 (2008).
159. C. P. Wild and B. W. Stewart, *World Cancer Report 2014* (World Health Organization, 2014).
160. M. Tsuboi, A. Hayashi, N. Ikeda, H. Honda, Y. Kato, S. Ichinose, and H. Kato, "Optical coherence tomography in the diagnosis of bronchial lesions," Lung Cancer **49**(3), 387–394 (2005).
161. R. G. Michel, G. T. Kinasewitz, K. M. Fung, and J. I. Keddissi, "Optical coherence tomography as an adjunct to flexible bronchoscopy in the diagnosis of lung cancer: a pilot study," Chest **138**(4), 984–988 (2010).
162. Y. Chen, M. Ding, W. J. Guan, W. Wang, W. Z. Luo, C. H. Zhong, M. Jiang, J. H. Jiang, Y. Y. Gu, S. Y. Li, and N. S. Zhong, "Validation of human small airway measurements using endobronchial optical coherence tomography," Respir. Med. **109**(11), 1446–1453 (2015).
163. M. Ding, Y. Chen, W. J. Guan, C. H. Zhong, M. Jiang, W. Z. Luo, X. B. Chen, C. L. Tang, Y. Tang, Q. M. Jian, W. Wang, S. Y. Li, and N. S. Zhong, "Measuring airway remodeling in patients with different COPD staging using endobronchial optical coherence tomography," Chest **150**(6), 1281–1290 (2016).
164. H. O. Coxson, B. Quiney, D. D. Sin, L. Xing, A. M. McWilliams, J. R. Mayo, and S. Lam, "Airway wall thickness assessed using computed tomography and optical coherence tomography," Am. J. Respir. Crit. Care Med. **177**(11), 1201–1206 (2008).
165. M. Kirby, K. Ohtani, T. Nickens, R. M. Lisbona, A. M. Lee, T. Shaipanich, P. Lane, C. MacAulay, S. Lam, and H. O. Coxson, "Reproducibility of optical coherence tomography airway imaging," Biomed. Opt. Express **6**(11), 4365–4377 (2015).
166. M. Kirby, K. Ohtani, R. M. Lopez Lisbona, A. M. Lee, W. Zhang, P. Lane, N. Varfolomeva, L. Hui, D. Ionescu, H. O. Coxson, C. MacAulay, J. M. FitzGerald, and S. Lam, "Bronchial thermoplasty in asthma: 2-year follow-up using optical coherence tomography," Eur. Respir. J. **46**(3), 859–862 (2015).
167. H. Pahlevaninezhad, A. M. Lee, A. Ritchie, T. Shaipanich, W. Zhang, D. N. Ionescu, G. Hohert, C. MacAulay, S. Lam, and P. Lane, "Endoscopic Doppler optical coherence tomography and autofluorescence imaging of peripheral pulmonary nodules and vasculature," Biomed. Opt. Express **6**(10), 4191–4199 (2015).
168. D. C. Adams, L. P. Hariri, A. J. Miller, Y. Wang, J. L. Cho, M. Villiger, J. A. Holz, M. V. Szabari, D. L. Hamilos, R. Scott Harris, J. W. Griffith, B. E. Bouma, A. D. Luster, B. D. Medoff, and M. J. Suter, "Birefringence microscopy platform for assessing airway smooth muscle structure and function in vivo," Sci. Transl. Med. **8**(359), 359ra131 (2016).

Biomedical Optics EXPRESS

169. A. M. Lee, K. Ohtani, C. Macaulay, A. McWilliams, T. Shaipanich, V. X. Yang, S. Lam, and P. Lane, "In vivo lung microvasculature visualized in three dimensions using fiber-optic color Doppler optical coherence tomography," J. Biomed. Opt. **18**(5), 050501 (2013).
170. H. Pahlevaninezhad, A. M. Lee, G. Hohert, S. Lam, T. Shaipanich, E. L. Beaudoin, C. MacAulay, C. Boudoux, and P. Lane, "Endoscopic high-resolution autofluorescence imaging and OCT of pulmonary vascular networks," Opt. Lett. **41**(14), 3209–3212 (2016).
171. J. Schmidbauer, M. Remzi, T. Klatte, M. Waldert, J. Mauermann, M. Susani, and M. Marberger, "Fluorescence cystoscopy with high-resolution optical coherence tomography imaging as an adjunct reduces false-positive findings in the diagnosis of urothelial carcinoma of the bladder," Eur. Urol. **56**(6), 914–919 (2009).
172. E. V. Zagaynova, O. S. Streltsova, N. D. Gladkova, L. B. Snopova, G. V. Gelikonov, F. I. Feldchtein, and A. Morozov, "In vivo optical coherence tomography feasibility for bladder disease," J. Urol. **167**(3), 1492–1496 (2002).
173. Z. Wang, C. S. Lee, W. C. Waltzer, J. Liu, H. Xie, Z. Yuan, and Y. Pan, "In vivo bladder imaging with microelectromechanical-systems-based endoscopic spectral domain optical coherence tomography," J. Biomed. Opt. **12**(3), 034009 (2007).
174. A. C. Goh, N. J. Tresser, S. S. Shen, and S. P. Lerner, "Optical coherence tomography as an adjunct to white light cystoscopy for intravesical real-time imaging and staging of bladder cancer," Urology **72**(1), 133–137 (2008).
175. N. Gladkova, E. Kiseleva, O. Streltsova, N. Prodanets, L. Snopova, M. Karabut, E. Gubarkova, and E. Zagaynova, "Combined use of fluorescence cystoscopy and cross-polarization OCT for diagnosis of bladder cancer and correlation with immunohistochemical markers," J. Biophotonics **6**(9), 687–698 (2013).
176. E. Kiseleva, M. Kirillin, F. Feldchtein, A. Vitkin, E. Sergeeva, E. Zagaynova, O. Streltzova, B. Shakhov, E. Gubarkova, and N. Gladkova, "Differential diagnosis of human bladder mucosa pathologies in vivo with cross-polarization optical coherence tomography," Biomed. Opt. Express **6**(4), 1464–1476 (2015).
177. M. T. Bus, B. G. Muller, D. M. de Bruin, D. J. Faber, G. M. Kamphuis, T. G. van Leeuwen, T. M. de Reijke, and J. J. de la Rosette, "Volumetric in vivo visualization of upper urinary tract tumors using optical coherence tomography: a pilot study," J. Urol. **190**(6), 2236–2242 (2013).
178. M. T. Bus, D. M. de Bruin, D. J. Faber, G. M. Kamphuis, P. J. Zondervan, M. P. Laguna-Pes, T. G. van Leeuwen, T. M. de Reijke, and J. J. de la Rosette, "Optical coherence tomography as a tool for in vivo staging and grading of upper urinary tract urothelial carcinoma: a study of diagnostic accuracy," J. Urol. **196**(6), 1749–1755 (2016).
179. M. Aron, J. H. Kaouk, N. J. Hegarty, J. R. Colombo, Jr., G. P. Haber, B. I. Chung, M. Zhou, and I. S. Gill, "Second prize: preliminary experience with the Niris optical coherence tomography system during laparoscopic and robotic prostatectomy," J. Endourol. **21**(8), 814–818 (2007).
180. F. Feldchtein, G. Gelikonov, V. Gelikonov, R. Kuranov, A. Sergeev, N. Gladkova, A. Shakhov, N. Shakhova, L. Snopova, A. Terent'eva, E. Zagainova, Y. Chumakov, and I. Kuznetzova, "Endoscopic applications of optical coherence tomography," Opt. Express **3**(6), 257–270 (1998).
181. L. P. Hariri, G. T. Bonnema, K. Schmidt, A. M. Winkler, V. Korde, K. D. Hatch, J. R. Davis, M. A. Brewer, and J. K. Barton, "Laparoscopic optical coherence tomography imaging of human ovarian cancer," Gynecol. Oncol. **114**(2), 188–194 (2009).
182. P. Molander, P. Finne, J. Sjöberg, J. Sellors, and J. Paavonen, "Observer agreement with laparoscopic diagnosis of pelvic inflammatory disease using photographs," Obstet. Gynecol. **101**(5 Pt 1), 875–880 (2003).
183. M. Kirillin, O. Panteleeva, E. Yunusova, E. Donchenko, and N. Shakhova, "Criteria for pathology recognition in optical coherence tomography of fallopian tubes," J. Biomed. Opt. **17**(8), 081413 (2012).
184. J. A. Burns, "Optical coherence tomography: imaging the larynx," Curr. Opin. Otolaryngol. Head Neck Surg. **20**(6), 477–481 (2012).
185. M. Rubinstein, E. L. Fine, A. Sepehr, W. B. Armstrong, R. L. Crumley, J. H. Kim, Z. Chen, and B. J. Wong, "Optical coherence tomography of the larynx using the Niris system," J. Otolaryngol. Head Neck Surg. **39**(2), 150–156 (2010).
186. M. L. Kaiser, M. Rubinstein, D. E. Vokes, J. M. Ridgway, S. Guo, M. Gu, R. L. Crumley, W. B. Armstrong, Z. Chen, and B. J. Wong, "Laryngeal epithelial thickness: a comparison between optical coherence tomography and histology," Clin. Otolaryngol. **34**(5), 460–466 (2009).
187. S. Guo, R. Hutchison, R. P. Jackson, A. Kohli, T. Sharp, E. Orwin, R. Haskell, Z. Chen, and B. J. Wong, "Office-based optical coherence tomographic imaging of human vocal cords," J. Biomed. Opt. **11**(3), 030501 (2006).
188. L. Yu, G. Liu, M. Rubinstein, A. Saidi, B. J. Wong, and Z. Chen, "Office-based dynamic imaging of vocal cords in awake patients with swept-source optical coherence tomography," J. Biomed. Opt. **14**(6), 064020 (2009).
189. A. M. Klein, M. C. Pierce, S. M. Zeitels, R. R. Anderson, J. B. Kobler, M. Shishkov, and J. F. de Boer, "Imaging the human vocal folds in vivo with optical coherence tomography: a preliminary experience," Ann. Otol. Rhinol. Laryngol. **115**(4), 277–284 (2006).
190. J. A. Burns, K. H. Kim, J. F. deBoer, R. R. Anderson, and S. M. Zeitels, "Polarization-sensitive optical coherence tomography imaging of benign and malignant laryngeal lesions: an in vivo study," Otolaryngol. Head Neck Surg. **145**(1), 91–99 (2011).

Biomedical Optics EXPRESS

191. J. A. Garcia, F. Benboujja, K. Beaudette, R. Guo, C. Boudoux, and C. J. Hartnick, "Using attenuation coefficients from optical coherence tomography as markers of vocal fold maturation," Laryngoscope **126**(6), E218–E223 (2016).
192. J. Jing, J. Zhang, A. C. Loy, B. J. F. Wong, and Z. Chen, "High-speed upper-airway imaging using full-range optical coherence tomography," J. Biomed. Opt. **17**(11), 110507 (2012).
193. J. Armstrong, M. Leigh, I. Walton, A. Zvyagin, S. Alexandrov, S. Schwer, D. Sampson, D. Hillman, and P. Eastwood, "In vivo size and shape measurement of the human upper airway using endoscopic longrange optical coherence tomography," Opt. Express **11**(15), 1817–1826 (2003).
194. J. J. Armstrong, M. S. Leigh, D. D. Sampson, J. H. Walsh, D. R. Hillman, and P. R. Eastwood, "Quantitative upper airway imaging with anatomic optical coherence tomography," Am. J. Respir. Crit. Care Med. **173**(2), 226–233 (2006).
195. L. Chou, A. Batchinsky, S. Belenkiy, J. Jing, T. Ramalingam, M. Brenner, and Z. Chen, "In vivo detection of inhalation injury in large airway using three-dimensional long-range swept-source optical coherence tomography," J. Biomed. Opt. **19**(3), 036018 (2014).
196. V. Volgger, G. K. Sharma, J. C. Jing, Y.-S. A. Peaks, A. C. Loy, F. Lazarow, A. Wang, Y. Qu, E. Su, Z. Chen, G. S. Ahuja, and B. J. Wong, "Long-range Fourier domain optical coherence tomography of the pediatric subglottis," Int. J. Pediatr. Otorhinolaryngol. **79**(2), 119–126 (2015).
197. C. T. Nguyen, W. Jung, J. Kim, E. J. Chaney, M. Novak, C. N. Stewart, and S. A. Boppart, "Noninvasive in vivo optical detection of biofilm in the human middle ear," Proc. Natl. Acad. Sci. U.S.A. **109**(24), 9529–9534 (2012).
198. H. R. Djalilian, J. Ridgway, M. Tam, A. Sepehr, Z. Chen, and B. J. Wong, "Imaging the human tympanic membrane using optical coherence tomography in vivo," Otol. Neurotol. **29**(8), 1091–1094 (2008).
199. G. L. Monroy, P. Pande, R. L. Shelton, R. M. Nolan, D. R. Spillman, Jr., R. G. Porter, M. A. Novak, and S. A. Boppart, "Non-invasive optical assessment of viscosity of middle ear effusions in otitis media," J. Biophotonics published ahead of print (2016).
200. A. Burkhardt, J. Walther, P. Cimalla, M. Mehner, and E. Koch, "Endoscopic optical coherence tomography device for forward imaging with broad field of view," J. Biomed. Opt. **17**(7), 071302 (2012).
201. Z. Hubler, N. D. Shemonski, R. L. Shelton, G. L. Monroy, R. M. Nolan, and S. A. Boppart, "Real-time automated thickness measurement of the in vivo human tympanic membrane using optical coherence tomography," Quant. Imaging Med. Surg. **5**(1), 69–77 (2015).
202. E. Guder, E. Lankenau, F. Fleischhauer, H. Schulz-Hildebrandt, G. Hüttmann, H. W. Pau, and T. Just, "Microanatomy of the tympanic membrane in chronic myringitis obtained with optical coherence tomography," Eur. Arch. Otorhinolaryngol. **272**(11), 3217–3223 (2015).
203. P. Pande, R. L. Shelton, G. L. Monroy, R. M. Nolan, and S. A. Boppart, "A mosaicking approach for in vivo thickness mapping of the human tympanic membrane using low coherence interferometry," J. Assoc. Res. Otolaryngol. **17**(5), 403–416 (2016).
204. W. Jung, J. Kim, M. Jeon, E. J. Chaney, C. N. Stewart, and S. A. Boppart, "Handheld optical coherence tomography scanner for primary care diagnostics," IEEE Trans. Biomed. Eng. **58**(3), 741–744 (2011).
205. D. MacDougall, J. Farrell, J. Brown, M. Bance, and R. Adamson, "Long-range, wide-field swept-source optical coherence tomography with GPU accelerated digital lock-in Doppler vibrography for real-time, in vivo middle ear diagnostics," Biomed. Opt. Express **7**(11), 4621–4635 (2016).
206. U. Mahmood, J. Ridgway, R. Jackson, S. Guo, J. Su, W. Armstrong, T. Shibuya, R. Crumley, Z. Chen, and B. Wong, "In vivo optical coherence tomography of the nasal mucosa," Am. J. Rhinol. **20**(2), 155–159 (2006).
207. A. Meller, M. Shakhova, Y. Rilkin, A. Novozhilov, M. Kirillin, and A. Shakhov, "Optical coherence tomography in diagnosing inflammatory diseases of ENT," Photonics Lasers Med. **3**(4), 323–330 (2014).

1. Introduction

Optical coherence tomography (OCT) is an imaging modality capable of obtaining images of tissue reflectance as a function of depth and transverse location on the sample. With a typical axial resolution of 10 μm and lateral resolution of 30 μm, these cross-sectional images provide unique information on microscopic architectural morphology. Another advantage of OCT is that it is a non-contact imaging modality. This characteristic has made it convenient to apply OCT in the eye, where it has become the gold standard for imaging retinal morphology and has further gained significant traction for anterior segment investigation. OCT has also been utilized to good effect for imaging the skin over large areas, providing similar information about the extent and depth of lesions [1–3].

These external clinical applications of OCT likely represent the "tip of the iceberg" as there is tremendous opportunity for disease diagnosis if this technology could be utilized inside the body. One irrefutable concept in medicine is that cancer could essentially be cured if it were detected and treated at an early stage before it has metastasized. The vast majority of these cancers arise from epithelial surfaces that line the internal organs of the gastrointestinal, pulmonary, ductal, gynecologic, and urothelial tracts, among others. Right

Biomedical Optics EXPRESS

now, the gold standard for early diagnosis is video endoscopy/bronchoscopy/laparoscopy with biopsy of visually suspicious lesions. Since these lesions are far to often below the resolution of endoscopy and frequently reside underneath the epithelial surface, the gold standard often falls short as an early detection modality. Were OCT to be developed as endoscopic probes and used to obtain microscopic images entire luminal organs, then possibly these pre-malignant or early stage cancers could be detected when curative interventions could be deployed. This opportunity is not limited to luminal organs, as probes can be utilized during laparoscopy to achieve the same affect.

Another important potential role of OCT is to obtain histomorphologic information for tissues that cannot be easily visualized or safely biopsied. A good example of this scenario is in the coronary arterial system where, prior to OCT, interventional guidance was based on silhouettes of the lumen via angiography or low resolution cross-sectional images provided by intravascular ultrasound (IVUS). OCT, with its capability to visualize microscopic architectural features, could change the precision with which clinicians intervene and could better determine which atherosclerotic plaques to treat. These same principles apply to other organs that cannot be easily or safely biopsied, such as the brain and pancreas.

Recognizing the potential benefits of obtaining these images in internal organ systems, investigators have spent the past 20 years developing OCT probes that can be inserted into the body. The earliest such probe was based on a rotationally scanning paradigm similar to that used in IVUS [4]. The distal optics in these probes both focus the beam and redirect it perpendicularly to the probe's long axis. This device obtains circumferential cross-sectional images by spinning the sample arm's focusing optics within a transparent sheath. Commonly the optical fiber that delivers light to the distal optics is enclosed within a driveshaft or wound cable that uniformly conveys torque from the proximal to distal portions of the probe. These types of devices also require optical rotary junctions to couple light from a fixed optical fiber emanating from the OCT system to a rotating optical fiber within the probe. As FD-OCT techniques have become popular, owing to higher speed and sensitivity, the driveshafts in many probes are now also used for translating the probe along the axis in addition to rotating. This so-called helical scan paradigm is now commonplace for endoscopic OCT, enabling three-dimensional imaging of long swaths of internal luminal organs [4–7]. An additional more recent advance replaces the rotary junction-driveshaft paradigm with a micro-motor at the distal tip of the catheter [8–14]. Such techniques have the advantage that kinks in the probe do not affect the rotational scan; resultant images have less binding artifacts than driveshaft-based designs [15].

While the helical scanning technique is common and comprises the majority of clinical endoscopic OCT devices, some applications mandate scanning along different planes within tissue [16]. Linear scanning OCT probes of a similar design that do not require optical rotary junctions have been utilized to obtain single cross-sectional images within the body [17–19]. Some applications such as imaging the bladder, cervix, myocardium, stomach, etc. require forward scanning systems [20, 21]. Endoscopic techniques for forward imaging have been implemented using fiber scanning systems, MEMS scanning mirrors, Risley scanners, etc [22–26].

2. Development of OCT endoscopes

Owing to strong optical attenuation (often dominated by scattering), OCT imaging depth in highly scattering tissues is limited to ~1-2.5 mm when a near infrared light source (800 – 1300 nm) is used, making it perfect for evaluating superficial tissues but impossible for directly accessing internal organs from outside the body. An OCT endoscope (or catheter) becomes a critical component for enabling OCT imaging of internal organs. In this review paper, we will focus on flexible, fiber-optic OCT endoscopes.

The basic function of an OCT endoscope is to deliver and focus an imaging beam on to a sample, scan the beam, collect the backreflected light from the sample, and transmit it back to

Biomedical Optics EXPRESS

the OCT interferometer. Since the first report of a fiber-optic scanning OCT endoscope/catheter 20 years ago [4], many different types of OCT endoscopes have been developed and demonstrated. Figure 1 illustrates some designs, which in essence include a single-mode fiber for beam delivery (e.g., SMF28e when using a 1300 nm source), micro optics to focus (and deflect) the beam, and a beam scanning device. Based on the direction of the imaging beam with respect to the longitudinal axis of the probe, OCT endoscopes can be divided into side-viewing endoscopes (Fig. 1(A)) and forward-viewing endoscopes (Fig. 1(B)). A side-viewing endoscope is more suited for surveying a large area of a luminal organ, while a forward-viewing endoscope is generally more suited for image guidance of biopsies, device placement, or treatments in which a sufficient space between the OCT probe and the sample surface is needed. The distal-end optics is often housed in a metal guard, and the entire fiber is encased in a torque coil that offers protection and flexibility. It can also transfer torque (for probe rotation) and allows for linear translation (for probe pullback) from the proximal end to the distal end. For practical use, the entire OCT endoscope is further encased in a transparent plastic sheath, which protects the probe from direct contact with body fluids and can be conveniently disinfected for human use. Based on the location of the beam scanning device, OCT endoscopes can be divided into proximal-end scanning probes (Fig. 1(C)) and distal-end scanning probes (see Fig. 1(D)). Proximal-scanning probes are more economical to engineer and often are compact, while distal-scanning probes offer much higher beam scanning speeds and minimize bending/stress-induced refractive index variations in a rotating fiber, and thus minimize distortion of OCT signals. Some advantages and disadvantages of the proximal- and distal-scanning endoscopes are summarized in Table 1.

Table 1. Summary of pros and cons of proximal- and distal-scanning endoscopes

Scanning Type	Min Probe Dia. and Rigid Length	Max Speed	Imaging Area	Fiber Stress-induced Distortion	Expense
Proximal-scanning	~0.5 mm (ϕ) ~1.0 cm (L)	~200 rps	Large (with pullback)	Moderate	Low (disposable)
Distal-scanning	~1.5 mm (ϕ) ~2.0 cm (L)	~4,000 rps	Large (with pullback)	Less	High (with micromotor)

2.1 Distal-end optics

Distal-end optics design in an OCT endoscope aims to achieve a desired focused beam spot size (i.e., lateral resolution) at a given working distance (i.e., the distance between the last surface of the optics to the focal point). One key constraint in the design is size, including the diameter and rigid length of the optics. A small diameter permits easy integration of the endoscope with existing clinical instruments (e.g., by passing the OCT probe through the 2.8 mm working channel of a gastroscope or a bronchoscope), while a short rigid length is required for the OCT probe to access small lumens through a potentially tortuous path (e.g., small airways) or pass through the Y-shape entry port of a clinical endoscope. A gradient index (GRIN) lens is often the preferred choice for the focusing element of an OCT endoscope owing to its compact size and cylindrical shape (which facilitates alignment and assembly of the distal-end optical components shown in Figs. 1(A)-1(D).

A simple and practical distal-end optics design is shown in Fig. 1(A), which includes a glass rod and a GRIN lens. For a side-viewing endoscope, a beam reflector is used to deflect the beam. Given the size constraint (normally about 1 mm in diameter), the optics design has to fully utilize the limited numerical aperture (NA) of the micro optics. Therefore, a glass rod (also called rod spacer) is often used to first expand the beam from the single-mode fiber (SMF) before it enters the GRIN lens. In this design two parameters, the length of the glass rod and the length of the GRIN lens, can be tuned to achieve the desired lateral resolution and working distance. Zemax simulations can be performed to determine the proper values of these two parameters for a target resolution and working distance. In practice, the simple

Biomedical Optics EXPRESS

ABCD matrix method for paraxial ray optics can be conveniently employed to generate quick estimates of the two control parameters and the trend of how the target parameters change versus the control ones. For a glass rod of a refractive index n_R and length z_R, and a GRIN lens of a refractive index profile $n(r) = n_{G0}\left(1 - \alpha^2 r^2 / 2\right)$ and a length z_G (where r is the distance from the optical axis of the GRIN lens, n_{G0} is the on-axis refractive index, and α is the refractive index profile constant and related the pitch number $P_\#$ of a GRIN lens by $P_\# = \alpha z_G / 2\pi$), we have the following ABCD matrix for the distal-end optics:

$$\begin{pmatrix} A & B \\ C & D \end{pmatrix} = \begin{pmatrix} 1 & d_w \\ 0 & 1 \end{pmatrix}\begin{pmatrix} 1 & 0 \\ 0 & n_{G0} \end{pmatrix}\begin{pmatrix} \cos(\alpha z_G) & \frac{1}{\alpha}\sin(\alpha z_G) \\ -\alpha \sin(\alpha z_G) & \cos(\alpha z_G) \end{pmatrix}\begin{pmatrix} 1 & 0 \\ 0 & \frac{n_R}{n_{G0}} \end{pmatrix}\begin{pmatrix} 1 & z_R \\ 0 & 1 \end{pmatrix}\begin{pmatrix} 1 & 0 \\ 0 & \frac{n_F}{n_R} \end{pmatrix} \quad (1)$$

Here n_F is the index of refraction of the SMF and d_w is the working distance. The matrices in Eq. (1) from the right to the left respectively represent (1) refraction at the SMF-glass rod interface, (2) propagation within the glass rod, (3) refraction at the glass rod – GRIN lens interface, (4) propagation within the GRIN lens, (5) refraction at the GRIN lens – air interface, and (6) propagation in air. The working distance d_w can be found from the image-forming condition $B = 0$. The focused spot size will be given by $\Delta x = AD_0$, where D_0 is the mode-field diameter of the SMF (and $D_0 \approx 9.2$ μm for the commonly used SMF28e +). The beam focus is generally set at about a few hundred microns outside the protective transparent plastic sheath, and thus the working distance is pre-determined. The optimal lateral resolution can then be found by tuning the length of the glass rod z_R and the length of the GRIN lens z_G.

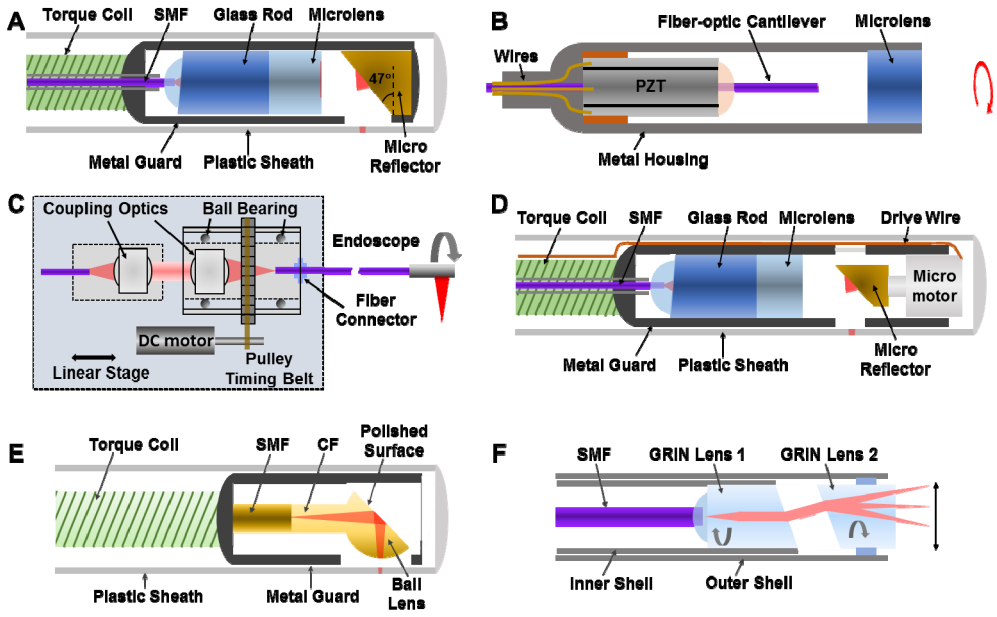

Fig. 1. Schematics of (A) Side-viewing OCT endoscope; (B) Forward-viewing endoscope; (C) Proximal scanning with a fiber-optic rotary joint. 3D imaging is performed by pulling back the rotating endoscope; (D) Distal-scanning endoscope with a micromotor; (E) Monolithic all-fiber-optic micro endoscope; (F) Pairs-angle-rotation-scanning forward-viewing endoscope. PZT: Lead zirconate titanate; SMF: single-mode fiber; CF: coreless fiber.

Biomedical Optics EXPRESS

When fabricating the endoscope, special care needs to be taken in order to minimize backreflection. A few embodiments can be implemented for the distal-end optics design. One is to have an 8-degree angle-cleaved end surface of the SMF and an 8-degree angle-polished entry surface of the glass rod (see Fig. 1(A)). These two surfaces remain parallel in the endoscope and can be joined together by UV curing optical cement. The separation between these two parallel surfaces can also be slightly adjusted to fine-tune the working distance and beam shape before UV curing. The glass rod can then by joined with the GRIN lens again by UV curing optical cement. The second embodiment is to have a non-45° tilting angle for the reflector in order to mitigate specular backreflection from the probe sheath or sample surface. In practice an approximately 47° (or 43°) tilt angle is sufficient which can deviate the specular reflection from the optical axis of the GRIN lens by 8 degrees. Another important parameter is the maximum beam diameter within the GRIN lens, which, as a rule of thumb, should be kept at less than 80% of the GRIN lens diameter in order to avoid beam clipping and transmission loss [27].

The above GRIN lens based OCT endoscope design offers great flexibility for controlling the focused beam spot size and working distance. However, it is difficult to fabricate small endoscopes by using a small GRIN lens (e.g., with a diameter of 250 μm or 350 μm). A novel monolithic all fiber-optic approach has been proposed and demonstrated for fabricating miniature OCT endoscopes [28–30]. Figure 1(E) illustrates the design schematic, in which an SMF is first thermally fused with a glass rod of the same or similar diameter (e.g., a multimode or coreless fiber). A ball lens can then be fabricated at the end of the glass rod through thermal arc melting (e.g., using a Fusion splicer), and the ball lens diameter (which determines its focusing power) can be fine-tuned through the arc parameters (such as the discharge temperature and duration). The focused beam spot size and the working distance are then determined by the glass rod length and the ball lens diameter. For side-viewing imaging, the ball lens can be polished at an angle (e.g., 47 degree or slightly larger to minimize specular backreflection). Total internal reflection at the polished surface can be utilized (e.g., with a 50-degree reflector angle) to deflect the beam for side-viewing imaging. An alternative (and more reliable) approach is to metallically coat the polished surface (e.g., 150 nm thick silver followed by 150 nm thick protective SiO) to ensure excellent reflection efficiency even when the probe is in direct contact with saline or body fluid in certain applications. It should be mentioned the fabrication parameters (such as the arc discharge temperature and duration) needs to be identified in a trial-and-error fashion for achieving the desired ball lens diameter (and shape) for a given fusion.

2.2 Scanning mechanisms

Side-viewing probes: For a side-viewing OCT endoscope, a scanning device can be placed either at the proximal end or the distal end. Most OCT endoscopes use proximal-end scanning, in which a fiber-optic rotary joint is used to couple light from a stationary source fiber to the rotating endoscope (see Fig. 1(C)) [5, 6, 10, 16, 31–39]. A rotary joint essentially consists of a pair of air-coupled lenses. The first one collimates the light from the source fiber and the second one focuses the collimated beam into the endoscope SMF (Fig. 1(C)). The first lens is fixed in space while the second one is mounted within a ball bearing that can be rotated by a DC motor. A quality rotary joint is expected to have a high throughput (> 85% one way) over the spectral range of interest, a low backreflection (< −55 dB), and a low variation in coupling efficiency during 360-degree rotation (< 10% peak to peak). For 1300 nm endoscopic OCT, a high-performance, compact fiber-optic rotary joint is commercially available (e.g., MJPP-LAPB-131-28-FA from Princetel Inc.), which can run at 150-200 rps (rotations per second), corresponding to an imaging speed of 150-200 circumferential frames/second.

For a side-viewing probe, beam scanning can also be performed by a micromotor placed at the distal end, which has a micro-reflector mounted on its shaft to deflect and scan the

Biomedical Optics EXPRESS

imaging beam (see Fig. 1(D)) [8–10, 40–42]. Distal-end scanning minimizes fiber bending/stress-induced changes in the refractive index as experienced in a proximal-scanning endoscope. As a result, distortion to OCT signals/images can be minimized. Two types of micromotors are commercially available, a DC micromotor (e.g., the ones from Namiki Inc. of a diameter as small as 0.9 mm and a rotation speed up to 200 rps) and an AC micromotor (e.g., the ones from Kinetron B.V. of a diameter as small as 1.0 mm and a rotation speed up to ~4,000 rps). Clearly, a higher imaging speed can be more easily achieved with a micromotor-based distal-scanning endoscope than a proximal-scanning endoscope. Recently intravascular "heartbeat" OCT imaging *in vivo* at a frame rate of 4,000 fps has been demonstrated with a distal-scanning probe along with a MHz FDML-based swept source [12]. One major challenge with a micromotor-based distal-scanning probe is its high cost (with a price tag of ~US$1,000-$2,000 per micromotor). In addition, micromotors are generally fragile, particularly AC micromotors which are highly sensitive to magnetizable materials and external magnetic fields. Although in principle it is possible to engineer a distal-scanning endoscope with a diameter smaller than 1 mm, in practice this is challenging and can be costly.

Owing to reduced stress-induced fluctuations in the refractive index within the fiber, distal-end scanning OCT endoscopes can offer a more stable interference signal than proximal-scanning probes, making them more suited for performing phase sensitive OCT imaging, including endoscopic angiography [14, 43, 44] and polarization-sensitive OCT [45, 46]. An alternative for improving the stability of endoscopic OCT interference signal is to employ common-path endoscopes [47, 48], in which both the sample and reference arms experience the same optical pathlength distortion in the fiber, leading to no net effect.

Forward-viewing probes: Forward-imaging endoscopes emit and collect light in the forward direction, i.e., along the longitudinal axis of the probe. Compared to a side-viewing probe, beam scanning represents a significant challenge in a flexible and compact forward-viewing endoscope. MEMS-based beam scanners are a natural choice, offering a stable and controllable scanning pattern at a high speed (e.g., in a few kHz range) through electrostatic or electrothermal actuations [49–51]. The drive voltage, generally in the range around one hundred volts, was a safety concern for *in vivo* applications; but MEMS technologies have evolved and the required drive voltage has dramatically reduced down to a few tens of volts to even a few volts by using thermal actuation [52–54]. The imaging beam within the endoscope, however, generally has to go through a folded path, resulting in a large probe diameter in the range of 4-5.8 mm, which remains a challenge in MEMS-based scanning endoscopes [49, 50, 52].

Generally speaking, a forward-viewing probe with a built-in beam scanner is more complicated to engineer than a side-viewing probe. The first fiber-optic forward-viewing scanning OCT endoscope was reported in 1997 [55]. The scanner was an electro-magnetic actuator, in which an optic-fiber mounted on a coil could be oscillated within a quadrupole magnetic field generated by two small permanent magnets when the coil was supplied with an AC current [56]. Light from the sweeping fiber tip was focused onto the sample by a microlens. An overall probe diameter of 2.2-2.7 mm was achieved with a scanning speed of 1 Hz up to a maximum of ~10 Hz. Another fiber-optic forward-viewing operating in the kHz range was based on a tubular PZT scanner (see Fig. 1(B)) [20, 57]. The high speed was achieved by inducing a resonant scanning mode of the fiber-optic cantilever when the PZT actuator was driven at the mechanical resonant frequency of the cantilever [58]. The resonant frequency is inversely proportional to the square of the cantilever length. As a rule of thumb, a 1-cm-long bare SMF28 fiber-optic cantilever corresponds to a resonant frequency of about 1 kHz. A scanning speed in the range of a few tens of Hz to a few kHz can then be conveniently achieved by choosing a proper cantilever length or by slightly modifying the cantilever diameter or mechanical modulus [59]. In addition to 1D scanning, 2D scanning in a spiral or Lissajous pattern has also been demonstrated [59, 60]. The overall probe diameter,

Biomedical Optics EXPRESS

governed by the diameter (1.2 – 1.5 mm) of the tubular PZT actuator, is about 2-2.4 mm, which is not very compact. Furthermore, the rigid length of the probe (about 3.5 cm including the imaging optics) is rather long. The rigid length can be further reduced to about 2.0 cm by using a shorter PZT tube, or by using a novel backward-mounting scheme [61]. Another novel beam scanning mechanism for a forward-viewing probe is the paired-angle-rotation scanner – PARS (see Fig. 1(F)) [62], in which a pair of angled-polished GRIN lenses are rotated in the opposite direction. A fan arc scan within a plane containing the optical axis (and thus a line scan projected on the tissue surface) can be achieved when the rotation of the GRIN lenses is of the same speed but in the opposite direction. Stable scanning requires that the two GRIN lenses retain excellent concentricity and stable separation during rotation, which can be challenging.

It should be mentioned that a forward-viewing OCT endoscope based on a coherent imaging fiber bundle has been reported [63]. The concept of using a fiber bundle was very attractive, because the imaging beam could then be conveniently scanned at the proximal end of the bundle and then transmit to the sample. However, the OCT signal and thus image quality were generally severely degraded by the multimoding within each individual core and by cross-talk among the cores that are simultaneously illuminated by the OCT beam [64–66], making this approach difficult to use in practice. In some special cases, such as angle-resolved low coherence interferometry (a/LCI) which is only concerned with the angular-dependent backscattering signal intensity rather than OCT images, a fiber bundle based endoscope is an excellent choice [67, 68].

3D volumetric imaging: In principle, 3D volumetric OCT imaging can be performed by any endoscopes capable of 1D beam scanning. For example, with a side-viewing probe, 3D volumetric data can be conveniently acquired by pulling back the 1D rotating probe (see Fig. 1(C)) along with the rotary joint with a linear stage [38, 69], in a similar fashion as in intravascular ultrasound imaging [70]. The separation between two adjacent circumferential (spiral) scans (i.e., the pitch along the rotation axis) can be easily controlled by the pullback speed. Similarly, 3D imaging can also be performed by an endoscope of a PZT-based 1D (line) along with pullback [71] or an endoscope of a PZT-based 2D scanner where pullback is not necessary [59].

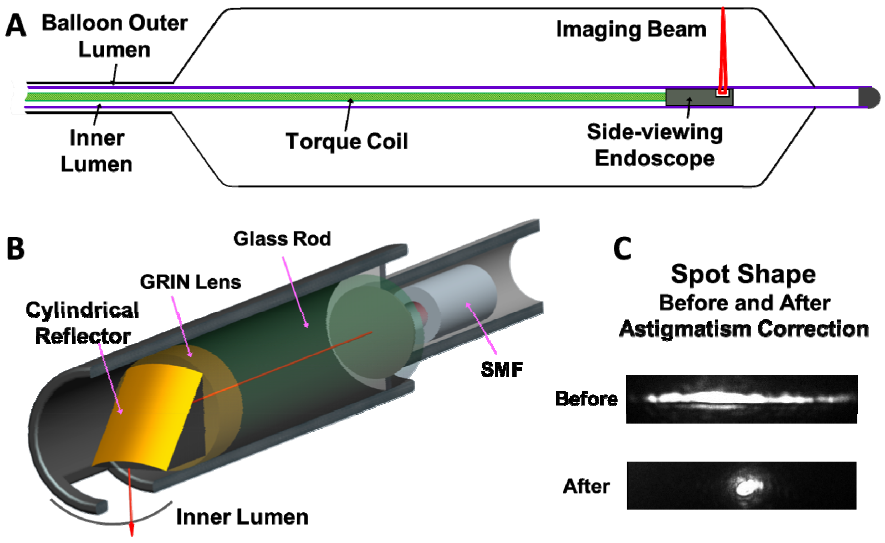

Fig. 2. (A) Schematic of a double-lumen OCT balloon endoscope; (B) Schematic of an OCT endoscope with astigmatism correction by introducing a cylindrical reflector. (C) Photos of focused spots before and after astigmatism correction. (Figure C adapted from [27].)

Biomedical Optics EXPRESS

2.3 Endoscopes for imaging large lumens

Balloon endoscope: When imaging a large lumen such as a human esophagus, extra challenges must be addressed in the OCT probe design, which includes needing a large working distance (e.g., 10-12 mm) and keeping the probe at the center of the lumen. A balloon endoscope has been developed to fulfil these needs [14, 72–74]. The schematic of a balloon endoscope is shown in Fig. 2(A), in which a side-viewing endoscope is placed within the inner lumen of a double-lumen balloon. For esophagus imaging, the balloon will be passed through the working channel of a standard gastroscope and then be inflated to stabilize the lumen and keep the endoscope in the center of the lumen. Thus both the OCT endoscope and the balloon need to have a small size. 3D imaging is again performed by pulling back a rotating OCT endoscope within the inner lumen while the balloon itself remains stationary. The distal-end optic design can basically follow the same idea as described in the section of *Distal-end optics*. In order to focus the beam 10-12 mm away from the center of the probe, one method is to employ a very thin (a few hundred microns) GRIN lens of a low focusing power. Care must be taken to accurately control the GRIN lens thickness since the focal position and the best achievable lateral resolution are highly sensitive to this parameter. An alternative is to employ a compound microlens, with the first lens to reduce the beam spot size from an SMF (e.g., by a factor of 2) and the second one of a decent thickness (1-2 mm) to gradually re-focus the beam to a target distance [27, 73]. This second approach offers more control for tuning the overall beam profile to achieve the best lateral resolution at the target working distance though it takes one extra step.

Another significant challenge in a balloon endoscope is the severe astigmatism. It is well known that a transparent plastic tube functions as a negative cylindrical lens, causing beam divergence along the azimuthal direction when passing through the tube wall from inside. The divergence is more pronounced for a working distance much larger than the radius of curvature of the tube surfaces. For a typical balloon catheter, an inner lumen of an about 1.5 mm diameter would significantly distort the beam shape, resulting in an ellipse (as opposed to a circle) with an ~40:1 aspect ratio at the working distance [27]. That means the lateral resolution along the azimuthal direction degrades by about 40 fold and the resulted circumferential OCT image would be effectively an average over multiple A-scans. One solution to this severe issue is to replace the commonly used flat reflector with a cylindrical reflector (Fig. 2(B)), which will pre-focus the beam along the azimuthal direction and compensate the divergence caused by the inner lumen of the balloon [27]. As shown the Reference [27], a diffraction-limited resolution of about 21 μm with a nearly round focused beam spot can be readily achieved at 11-mm working distance (Fig. 2(C)).

Biomedical Optics EXPRESS

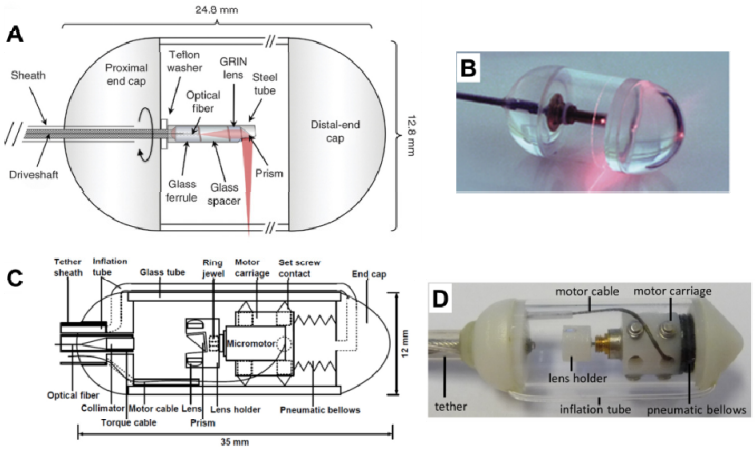

Fig. 3. (A) Schematic and (B) photo of a tethered proximal-scanning OCT capsule endoscope. (Figures A and B adapted from Ref [75].) (C) Schematic and (D) photo of a tethered distal-scanning OCT capsule. (Figures C and D adapted from [11].)

Tethered capsule endoscope: Although OCT balloon endoscopes offer excellent images of the esophagus over a large area, the procedure, similar to other clinical endoscopic ones, requires subject sedation and a specialized setting. A novel tethered OCT capsule endoscope has been recently developed to overcome this application hurdle [75]. The tethered capsule can be swallowed by a conscious patient and imaging can be, in principle, performed in a clinic without the need for sedation or a special setting. Figures 3(A) and 3(B) show a schematic and photo of the first prototype, respectively. The capsule had dimensions of 12.8 mm x 24.8 mm (diameter x length) with a side-viewing OCT endoscope placed in the middle of the capsule. Circumferential imaging at a speed of 20 frames/second with a resolution of 30 μm x 7 μm (lateral x axial in tissue) was performed on human subjects by rotating the endoscope through a fiber-optic rotary joint at the proximal end. The capsule was attached with a tether. 3D imaging data was acquired when the capsule was swallowed down the esophagus with the help of natural peristaltic force, or when the capsule was mechanically pulled backward via the tether. The size of the capsule (particularly the diameter) was carefully chosen so that it was able to be swallowed while the majority of esophagus epithelium remained in contact with the capsule surface without much folding. More recently an innovative distal-scanning tethered capsule was reported [11]. Beam scanning was achieved by a DC micromotor of a 4 mm diameter (Namiki Inc.), which spun a 90-degree reflector along with a focusing lens within the capsule (see Figs. 3(C) and 3(D)). The capsule had overall dimensions of 12 mm x 38 mm (diameter x length). The high-speed micromotor, along with a high-speed tunable VCSEL swept source of a 1 MHz A-scan rate, enabled ultrahigh-speed imaging at 250 frames/second with an imaging resolution of 26 μm x 8.5 μm (lateral x axial in tissue). One novel feature of this capsule design was its built-in miniature pneumatic bellows that could translate the micromotor-based beam scanner (along the capsule axis) for 3D imaging with a well-controlled speed (and pitch), making it possible to perform high-precision *en face* imaging.

Biomedical Optics EXPRESS

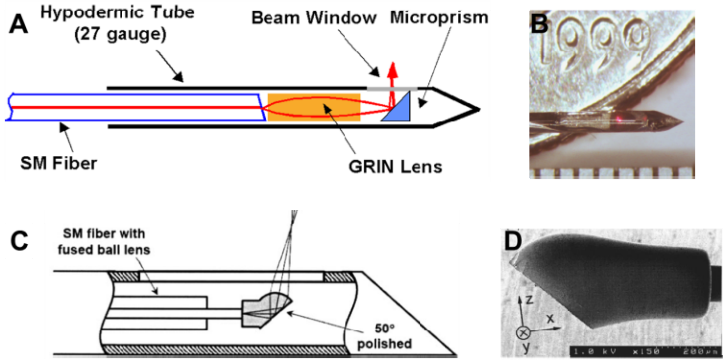

Fig. 4. (A) Schematic and (B) photo of an OCT imaging needle. (Figures A and B adapted from Ref [76].) (C) Schematic and (D) SEM micrograph of a monolithic ball lens-based OCT imaging needle. (Figures C and D adapted from [30])

2.4 Ultracompact OCT endoscopes and imaging needles

In contrast to a balloon or capsule endoscope for large lumen imaging, another technology push is an endoscope of an extremely compact size in order to (1) minimize the potential impact of the probe on the lumens and/or (2) access smaller lumens (such as small airways) [77]. By encasing the compact distal-end optics in a sharpened hypodermic tube, the probe becomes an imaging needle. An OCT needle probe enables interstitial imaging of solid organs beyond the conventional OCT imaging depth. The probe can be potentially integrated within an excisional biopsy needle to provide a "first look" of the target tissue, and guide biopsy to be taken from the most representative tissues (e.g., the most malignant tissue of cancer) for improving diagnostic yield. Figures 4(A) and 4(B) show the schematic and photo of the first prototype OCT imaging needle reported in 2000 [76], respectively, which consisted of a GRIN lens and a 45-degree rod reflector (both of a 250 μm diameter). Interstitial side-viewing imaging was performed by rotating the needle at a given insertion depth [76]. The initial distal optics design for the needle probe was tricky to assemble. An innovative monolithic approach (as discussed before) is a much preferred approach (see Figs. 4(C) and 4(D)) for fabricating a miniature imaging needle [30, 78–81].

To avoid direct contact of the fragile distal-end optics with biological tissues, the imaging needle or ultrathin probe is often encased in a transparent glass tube. The small glass tube, similar to the balloon inner lumen discussed previously, introduces severe astigmatism. Several approaches have been proposed to mitigate this adverse effect [78, 82, 83]. One way is to fill the glass tube with index matching fluid and make a flat beam window on the outer surface of the tube by polishing to remove the cylindrical lens effect [78]. Another approach is to design a ball lens (by thermal melting) to have an ellipsoidal shape with a smaller radius of curvature (and thus stronger focusing) along the azimuthal direction, which will pre-compensate the negative cylindrical lens effect [82].

2.5 Ultrahigh-resolution endoscopes

Most endoscopic OCT imaging thus far has been performed in the 1300 nm wavelength range. With recently developed advanced light sources, an axial resolution around 10 μm in air was achieved [14, 38, 69]. OCT axial resolution is governed by the center wavelength λ_0 and the spectral bandwidth $\Delta\lambda$ of the light source, i.e., $\Delta z = 2ln2\,\lambda_0^2/(\pi\Delta\lambda)$. The quadratic dependence of the axial resolution on the center wavelength suggests axial resolution can be effectively improved by using a low coherence source of a shorter center wavelength. Ultrahigh resolution (1.5 μm axial) was demonstrated on a bench-top OCT system with an 800 nm broadband light source (a short pulsed Ti:Sapphire laser of a 260 nm FWHM bandwidth). An additional benefit of imaging in the 800 nm wavelength range is the

Biomedical Optics EXPRESS

improvement on imaging contrast owing to stronger light scattering (and weaker absorption) at 800 nm than at 1300 nm. Ultrahigh-resolution endoscopic OCT imaging has long been of interest to the field. Among the many technical challenges in developing 800 nm ultrahigh-resolution OCT endoscopes, a significant one is managing the chromatic aberration in the micro optics so that all the wavelengths within the broad source spectrum can be equally focused along the imaging depth. Several prototypes of ultrahigh-resolution OCT endoscopes have been reported, including a side-viewing probe in which cross-sectional imaging was performed through pullback along the probe axis [84], and a forward-viewing probe where cross-sectional imaging was achieved by using a resonant fiber-optic PZT scanner [85]. In both cases, chromatic aberration was managed by customized multi-element miniature microlenses of a 2.0 mm diameter including the housing tube. The measured axial resolution was around 3.0 μm x 4.0 μm (axial x lateral in air) when a Ti:Sapphire laser of an ~150 FWHM spectral bandwidth was used. Despite the excellent resolution and promising potential, translational applications and wide acceptance of ultrahigh-resolution OCT endoscopy in the 800 nm wavelength range faced a prohibitive cost issue, since each super-achromatic microlens cost about US$10,000, and few vendors were willing to fabricate the micro compound lens (such as Bern Optics, Inc.). The cost is expected to be even higher if a super-achromatic microlens smaller than the reported ones (i.e., of 1 1.5-1.7 mm optics diameter) [84, 85] is needed for further reducing the overall 2-mm endoscope diameter.

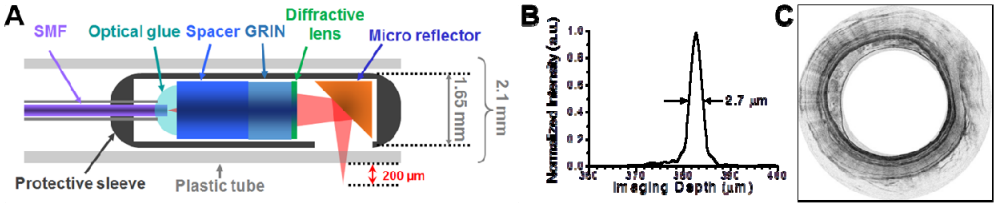

Fig. 5. (A) Schematic of a diffractive optics-based ultrahigh-resolution OCT endoscope. (B) Measured axial resolution afforded by the diffractive OCT endoscope. (C) Representative OCT image of a guinea pig esophagus *in vivo* acquired with the diffractive endoscope. (Figure A adapted from [7]; Figures B and C adapted from [86].)

Recently a novel approach has been developed by using diffractive optics [7, 86] (see Fig. 5(A)). The diffractive lens can be made small (1 mm or smaller) and is very cost effective. It can be conveniently used in conjunction with a GRIN lens and deviates each wavelength within the spectrum in the direction opposite to the direction caused by chromatic aberration. A super-achromatic endoscope with 1 mm diameter optics (1.3 mm overall diameter with the metal tube) and an excellent axial resolution of 2.7-3.0 μm (in air) and *in vivo* imaging quality were demonstrated (see Figs. 5(B) and 5(C)) [86]. Considering compact turn-key broadband light sources at 800 nm (e.g., the super-continuum source from NKT Photonics) are commercially available and their optimal operational conditions have also been reported (with resulted OCT imaging quality similar to that obtained with a short pulsed Ti:Sapphire laser) [86], ultrahigh-resolution OCT endoscopy is expected to translate to clinical practice in the near future.

2.6 Multimodal endoscopes

OCT imaging contrast is governed by tissue optical absorption and scattering properties (and in general dominated by scattering). It is naturally a label-free imaging technology. Arguably one limitation is the lack of molecular sensitivity, and another is the limited imaging depth. One solution is to combine OCT with other complementary spectroscopy or imaging technologies, including fluorescence or reflectance (for gaining molecular or chemical specificity) and ultrasound (for improving imaging depth). In the following we will briefly review the development of OCT-based multimodal endoscopy technologies.

Biomedical Optics EXPRESS

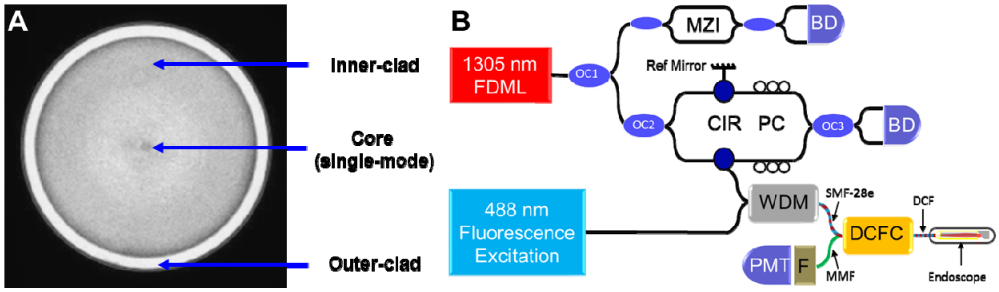

Fig. 6. (A) Photo of a double-clad fiber (DCF) end surface. (B) Schematic of a representative OCT-Fluorescence dual-modal endoscopic system. (Figure B adapted from [87.])

OCT and fluorescence imaging: Fluorescence excitation light can be delivered to the sample through the single-mode core of a conventional OCT endoscope; however, the core diameter (e.g., 9.3 μm for SMF28e) is too small to effectively collect fluorescence emission. Thus fluorescence imaging cannot be performed using a conventional OCT endoscope. Many innovative solutions have been proposed and demonstrated. In the first OCT-fluorescence dual-modal endoscope, the OCT imaging probe and the diffuse fluorescence spectroscopy probe were physically put together at the distal end within a fused-silica tube of a 2 mm diameter [88]. Cross-sectional OCT imaging (lateral x depth) and 1D fluorescence spectroscopy (no depth info) were performed by translating the probe in a push-pull mode. To minimize the probe size, a single-fiber based dual-modal probe was later developed [89], in which OCT and fluorescence shared the same double-clad fiber (DCF, see Fig. 6(A)) and microlens for light delivery and focusing. The single-mode core of the DCF (with an ~10 μm mode-field diameter) was used to transmit OCT light (1300 nm), while the multi-mode inner-cladding (of a 125 μm diameter) was used for transmit fluorescence excitation (488 nm) and emission (550 – 800 nm). The reported probe is a non-scanning probe and imaging was performed by physically moving the probe with a translation stage. Recently, a more advanced OCT-fluorescence endoscope was demonstrated, which had a side-viewing monolithic DCF-based probe (with distal-end optics similar to Fig. 1(E)) [90]. Real-time imaging (3D for OCT and 2D for fluorescence) at a speed of 25.4 frames/second was enabled by a custom built DCF rotary joint along with a pullback stage. *In vivo* intravascular OCT and fluorescence molecular imaging was performed on a rabbit model. The challenges with a DCF-based rotary joint include maintaining precision alignment during rotation and preventing the backscattered light at OCT wavelength in the probe's inner cladding from being coupled back to the OCT interferometer (which would otherwise distort OCT images owing to the different optical pathlengths). To avoid using a DCF rotary joint, distal-end scanning OCT-Fluorescence endoscopes were proposed [87,91], and a representative system schematic is shown in Fig. 6(B). One unique feature of the systems is the introduction of a special fiber-optic combiner (DCFC), which can effectively separate OCT light (single-mode, transmitting through the DCF core in the endoscope) and fluorescence light (multimode, transmitting through the DCF inner cladding). Such confiners have now become commercially available (e.g., from Thorlabs Inc.). Similar concepts have been implemented in a dual-modal imaging needle [92, 93]. It is also notable that the same dual-modal endoscopes/needles can also be used for OCT-Reflectance imaging. It is well known that the sensing depth of diffuse reflectance depends on the source-detector separation (approximately 1/2 of the source-detector separation) [94–96]. Thus, in order to gain rough depth sensitivity through the reflectance measurement, a double-probe approach can be used where OCT and reflectance share the same probe (and even the same broad band source) while reflectance collection is performed by a second probe [97]. In addition to single-photon fluorescence, two-photon fluorescence imaging at submicron resolution has also been integrated with OCT

Biomedical Optics EXPRESS

endoscopy, where a forward-viewing PZT-based DCF scanning endoscope was shared by both modalities [98].

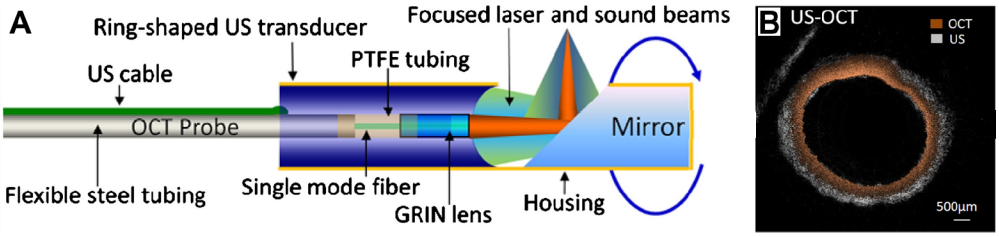

Fig. 7. (A) Schematic of an OCT-ultrasound dual-modal endoscope with two modalities sharing the same working distance and capable of co-registration. (B) Representative OCT image of a rabbit aorta *ex vivo* overlaid on the corresponding ultrasound image acquired with the dual-modal endoscope. (Figures adapted from [99], with the full permission of AIP publishing.)

OCT and ultrasound imaging: Recent years have seen increasing interest in integrating OCT with ultrasound in an endoscope setting, aiming to access tissues beyond the 1-2.5 mm OCT imaging depth. Early OCT-ultrasound dual-modal endoscopes adopted the same approach as the early OCT-fluorescence endoscope, in which a side-viewing OCT endoscope and an ultrasound endoscope were put side by side [100, 101]. With this approach, however, it is difficult to co-register OCT and ultrasound imaging beams (i.e., to share the same beam path or focus). A more elegant dual-modal endoscope design was later developed capable of co-registered OCT-Ultrasound imaging [99], in which a OCT probe of a 0.7 mm diameter passed through a 50 MHz ring ultrasound transducer (of a 2 mm diameter) via a 0.8 mm centric hole (see Fig. 7). Both OCT and ultrasound beams were deflected by a 45-degree mirror for side-viewing imaging, and a confocal length of 4 mm was achieved. The distal-end imaging optics and ultrasound transducer was encased in a brass tube with an outer diameter of 2.5 mm and a precut window for beam passage. Simultaneous circumferential OCT and ultrasound imaging were performed by rotating the entire probe with a fiber-optic rotary joint (for OCT) integrated with an electrical slip ring (for ultrasound) at the proximal end. For ultrasound imaging, the probe distal end was presumably submerged in saline. Excellent performance of the dual-modality endoscope was demonstrated on *ex vivo* imaging of rabbit aorta. It is anticipated that the probe diameter will be further reduced to facilitate *in vivo* applications. In addition to OCT-ultrasound dual-modality integration, prototypes of tri-modal endoscopes (OCT, ultrasound and photoacoustic) have recently been demonstrated [102, 103], enabling simultaneous, multi-resolution, multi-contrast and multi-scale imaging of internal organs.

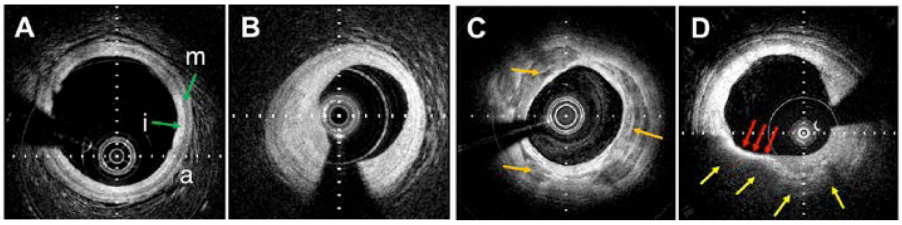

Fig. 8. OCT images of human coronary plaques *in vivo*. (A) Artery wall with intimal hyperplasia. (B) Fibrous plaque showing a thickened intima. (C) Calcific plaque demonstrating a heterogeneous, signal poor region (orange arrows) with clearly demarcated borders. (D) OCT fibroatheroma, showing a signal poor region with poorly defined borders (yellow arrows), consistent with lipid, and overlying tissue, known as the fibrous cap (red arrows). Tick marks in (A), (B), and (D) – 250 μm. Tick marks in (C) – 500 μm.

Biomedical Optics EXPRESS

3. Applications of endoscopic OCT in the clinic

3.1 Cardiovascular system

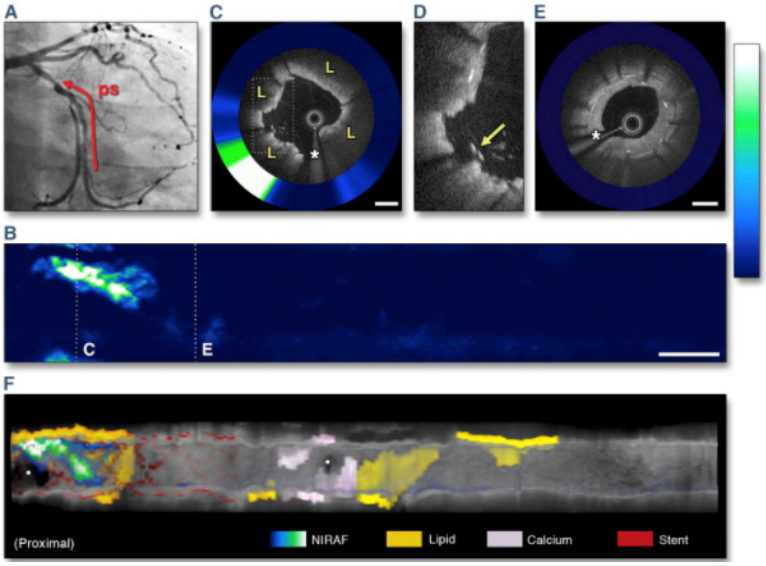

Fig. 9. Angiography of the left circumflex coronary artery (A) and 2-dimensional NIRAF map (B). (C) Cross-sectional OCT-NIRAF image and (D) magnified portion showing elevated NIRAF colocalized with stent struts overlying an OCT-delineated fibroatheroma. (E) Cross-sectional image from the distal portion of the stent that is negative for NIRAF. (F) Three-dimensional cutaway rendering with overlaid NIRAF signal. Scale bars on OCT images are equal to 1 mm; scale bar in (B) is equal to 5 mm. (∗) Indicates a guidewire shadow. ps = pullback segment; L = lipid. (Figure and caption adapted from [111], with permission from Elsevier.)

The diagnosis of intravascular disease is possibly the most advanced clinical application space for OCT other than ophthalmology. Multiple clinical OCT catheter devices are commercially available or under development for imaging coronary artery wall microstructure. Once the catheter is inserted into the artery, using a brief, 2-3 second saline or radiocontrast flush, blood is removed from the field, followed by a rapid helical scan of the OCT catheter's optics over a length of about 5-10 cm. Intravascular OCT imaging provides three-dimensional data on the detailed microstructure of the coronary wall that can be used to guide interventional procedures and provides information about the diagnosis of atherosclerotic lesions. The main advantage of OCT for imaging coronary atherosclerosis is its high resolution that enables the differentiation of many macro and microscopic features, including lipid [104], calcium [104], cholesterol crystals [105], thrombus [106], and accumulations of macrophages [107, 108] that enable the discrimination of plaque type (Fig. 8). The primary disadvantage of OCT for imaging coronary atherosclerosis is poor penetration depth when imaging through macrophages or lipid containing tissues, resulting in an inability to determine the volume extent of many lesions and challenges in image interpretation [109, 110].

To further improve OCT's capability to differentiate types of atherosclerotic lesions, first in human results were published with a dual-modality catheter that can simultaneously collect OCT and near-infrared autofluorescence (NIRAF) from the same location in the tissue [111]. A special rotary-junction enabled volumetric imaging with both modalities showing focal distribution of NIRAF signal corresponding to plaques with a high-risk morphological phenotype. These early results suggest that combining microstructural OCT data with NIRAF molecular/chemical information can improve the detection of high-risk plaques (Fig. 9).

Biomedical Optics EXPRESS

The current clinical application for intracoronary OCT is guidance of interventional procedures. While these procedures are generally safe and without complication, there is some estimated 5-10% of cases that result in adverse events such as in-stent restenosis, stent failure, or stent thrombosis [112, 113]. Many experts believe that improved visualization of the artery wall to guide stent placement will decrease the incidence of these adverse events. Ensuring that the stent completely covers the culprit lesion and the edge is not placed in the middle of a fibroatheroma should allow the artery to heal in an improved manner. Further, OCT can be used to determine if the stent is placed properly, avoiding malapposition (Fig. 10A) and large stent edge dissections (Fig. 10B) that could place the patient at risk for target lesion revascularization. Evidence is mounting for the benefits of using OCT to guide intervention [114–117] and seminal clinical trials to prove efficacy and improved patient outcomes are underway.

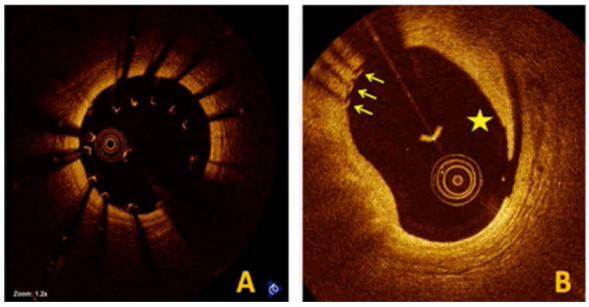

Fig. 10. Findings at stent implantation. (A) Under-expanded stent with malapposed struts. (B) Edge dissection flap (*star*) and stent struts (*arrows*) are observed. (Figure and caption adapted with permission of Springer from [118].)

Another intravascular application of OCT is the guidance of peripheral artery atherectomy procedures. A commercially available device has been introduced that combines OCT with a cutting blade in a single catheter. This technology allows the interventionalist to visualize the artery wall in detail to ensure that the blade does not cut completely through uninvolved artery and only removes plaque. Studies investigating this promising application of OCT have shown that the time to conduct peripheral atherectomy procedures is decreased and the complication rate is lower with OCT guidance [119].

3.2 Gastrointestinal tract

Esophagus: The most investigated application of OCT in the GI tract is the diagnosis of Barrett's Esophagus (BE), a premalignant transformation of normal squamous mucosa to glandular mucosa, caused by gastric reflux, near the distal portion of the esophagus (GEJ). This glandular mucosa can undergo neoplastic transformation to esophageal adenocarcinoma (EAC). EAC is usually detected at a late, symptomatic stage when the cancer has metastasized, resulting in a dismal 5-year survival rate of 15-20% [120]. Two problems exist in managing BE. First, most with BE do not know they have the condition, mandating some sort of screening paradigm. For those with BE, they must be followed (surveillance) to determine if they have developed dysplasia or early cancer so that they can be treated at an earlier, curative stage. The current standard of care, endoscopy with biopsy, is limited for both BE screening and surveillance because it is too expensive and cumbersome for screening and cannot readily identify dysplasia. Thus, those undergoing surveillance must be randomly biopsied, frequently missing the most severe disease foci.

Biomedical Optics EXPRESS

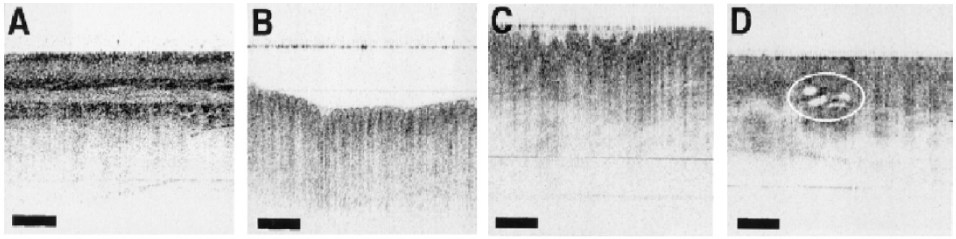

Fig. 11. (A) OCT image of normal squamous epithelium (bar = 500μm) shows a 5-layered appearance (from top to bottom: epithelium, lamina propria, muscularis mucosa, submucosa, and muscularis propria). (B) OCT image of gastric mucosa with "pit and crypt" architecture. (C) OCT image of BE with an irregular mucosal surface and absence of a layered or pit and crypt architecture. (D) OCT image of BE with submucosal glands (circled). (Figure and caption adapted from [121], with permission from Elsevier.)

The first investigations of OCT for BE utilized either linear driveshaft [17, 122] or fiber scanning probes [55] inserted into the accessory ports of endoscopes. Data acquired from these early studies showed that the architectural morphology seen by OCT enabled clear delineation of squamous mucosa from BE and stomach (gastric cardia) [121, 123, 124] (Fig. 11). Further studies also showed that OCT was capable of diagnosing dysplasia by using architectural analogs of the modified Haggitt criteria [125] (Montgomery criteria [126]) related to surface maturation and glandular atypia, employed by pathologists [127, 128]. While these initial studies showed promise for the OCT diagnosis of BE, the probes were limited to imaging limited discrete locations in the esophagus and therefore were subject to sampling error.

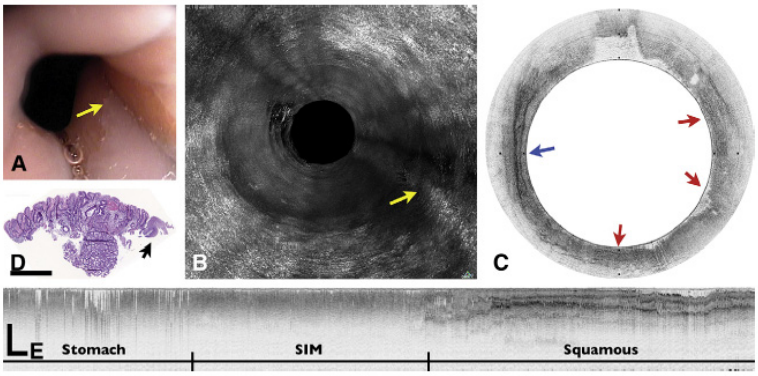

Fig. 12. Presumed Barrett's esophagus. (A) Videoendoscopic image shows an irregular SCJ with a tongue of healthy mucosa (arrow). (B) An MIP rendering of the entire volumetric OFDI data set, obtained at the corresponding location in A. (C) Corresponding cross-sectional OFDI image demonstrates squamous mucosa (blue arrow) interspersed with regions that satisfy the OCT criteria for BE (red arrows). (D) Histopathologic image of the biopsy specimen taken from the SCJ with no signs of intestinal metaplasia (H&E, orig. mag. 2). (E) A longitudinal OFDI cross-section through the SCJ shows a 12-mm segment of mucosa that is consistent with BE. Scale bars and tick marks represent 1 mm. (Figure and caption adapted from [129], with permission from Elsevier.)

The landscape for OCT esophageal imaging changed in the mid-2000's with the advent of SS-OCT [10, 37, 130] (also known as OFDI) and balloon centering esophageal catheters [38, 129]. The speed of SS-OCT and the centering capabilities of the balloon enabled comprehensive helical imaging (now known as volumetric laser endomicroscopy - VLE [131]) of the entire distal esophagus (Fig. 12) in realistic procedure times. By imaging the entire portion of the organ at risk, sampling error could in principle be eliminated.

Biomedical Optics EXPRESS

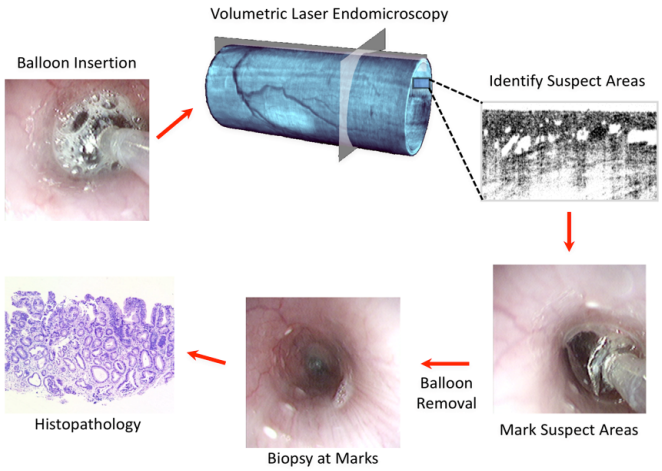

Fig. 13. Schematic of VLE-guided biopsy. (Figure and caption adapted from [132].)

The capability to visualize the entire distal esophagus on the microscopic scale opened the possibility of implementing OCT-targeted biopsy as opposed to random biopsy. This technique was demonstrated using superficial laser cautery [133]. The cautery light, also transmitted through the centering balloon probe's optical fiber, was at a different wavelength that was strongly absorbed by water. A schematic of the targeted biopsy paradigm is shown in Fig. 13. Briefly, a VLE image of the distal esophagus was acquired. Either after the 3D scan or during image acquisition a region suggested of dysplasia was identified, with the balloon still in place, the operator instructed the system to place down laser cautery marks in the patient's esophagus at the location at which the suspect image was acquired. Following the marking of suspicious locations, the balloon was removed from the patient and the clinician then biopsied near the marks. The histology matched the OCT image selected in real time from the patient. VLE [131] and laser marking are now commercially available and are being tested in clinical trials. Another approach for comprehensive imaging of the esophagus has been the utilization of an ultra-high speed form of SS-OCT that employs a Fourier Domain Mode-locked Laser (FDML) [134] or VCSEL [135] light source.

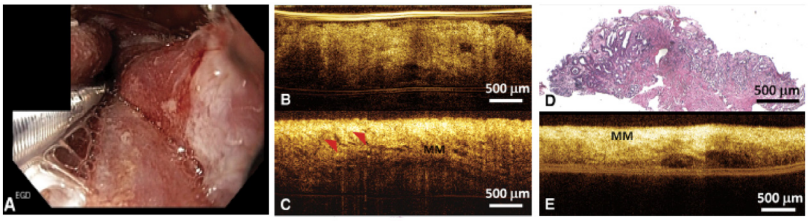

Fig. 14. A, Representative endoscopic image of the gastroesophageal junction immediately after radiofrequency ablation (RFA) treatment. B, Representative cross-sectional OCT image showing unburned Barrett's esophagus epithelium missed by RFA. C, Representative cross-sectional OCT image showing residual glands after RFA and D, corresponding histology confirming residual BE glands after RFA (H&E, orig. mag. x4). E, Representative cross-sectional OCT image showing effective RFA treatment. (Figure and caption adapted from [136], with permission from Elsevier.)

The unique capability of OCT to provide information about internal tissue structures has been employed to assess efficiency of radio-frequency ablation (RFA) of BE. Three-dimensional endoscopic OCT non-balloon probes were used to investigate the presence of buried glands beneath neo-squamous epithelium after RFA [130, 136]. Following the first case report [130], results from 32 patients with short BE segment were presented, showing

Biomedical Optics EXPRESS

that thinner epithelium and OCT-visible glands (Fig. 14) can be correlated with the presence of residual BE at follow-up after RFA treatment [136].

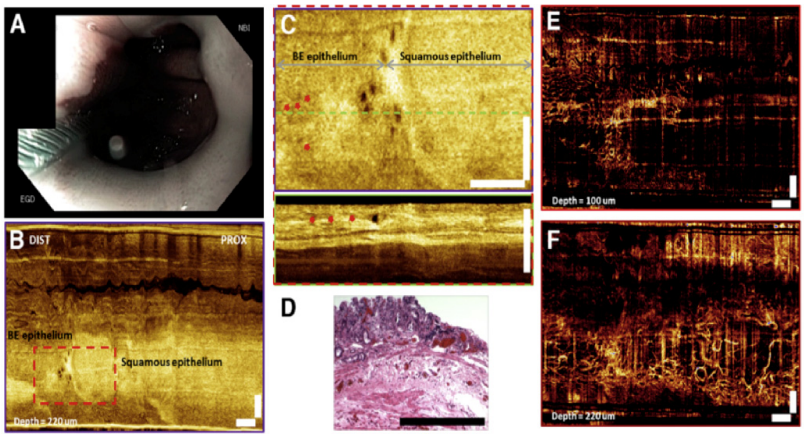

Fig. 15. (A) Endoscopic view of BE using narrow band imaging. (B) *En face* OCT image at 220 mm depth (lamina propria layer). (C) Enlarged *en face* OCT image and the corresponding cross-sectional OCT image and (D) histology from the dashed red region in (B). *En face* OCT angiograms: (E) at 100 mm depth showing surface vasculature in the BE region, and (F) at 220 mm depth showing high density of microvasculature along the squamocolumnar junction. Red arrows, BE glands; white bar, 1 mm. (Figure and caption adapted from [44], with permission from Elsevier.)

The first endoscopic two-dimensional Doppler OCT images, obtained with a linear scanning side-viewing probe, showed different microcirculation patterns in normal and diseased tissues in the human digestive system [36]. Investigators have recently combined VCSEL-based OCT systems with endoscopic probes that incorporate scanning micro-motors to obtain detailed three-dimensional views of BE architecture and blood flow (Fig. 15) [10, 44, 137]. This volumetric OCT opens new possibilities for obtaining additional features that may improve the diagnosis of BE. Blinded analysis of abnormal microvasculature in OCTA data obtained in 41 patients showed 94% sensitivity and 69% specificity for differentiating LGD/HGD from non–dysplastic BE [138].

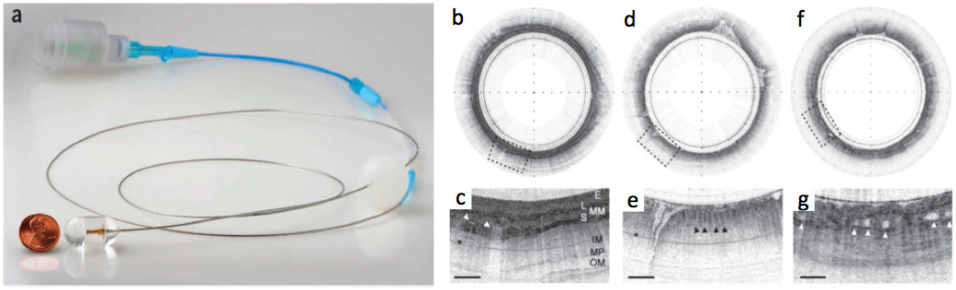

Fig. 16. (a) Tethered capsule endomicroscopy (TCE) device. TCE images obtained from a healthy volunteer *in vivo*: (b, c) in the normal esophagus (squamous epithelium (E), muscularis mucosa (MM), lamina propria (L), submucosa (S) containing blood vessels (arrowheads), inner muscularis (IM), outer muscularis (OM) and myenteric plexus (MP)), and (d, e) in the stomach showing characteristic glandular 'pits' (arrowheads). (f, g) TCE image obtained from a patient with BE *in vivo*. The asterisks indicate a multiple reflection artifact. Tick marks, (b, d, f) 1 mm; scale bars, (c, e, g) 0.5 mm. (Figure and caption adapted from [75].)

While these high speed, three-dimensional imaging forms of OCT have shown promise for improving surveillance of those with BE, there remains a problem of identifying the many patients with BE who are not diagnosed. This clinical dilemma motivated the development of

Biomedical Optics EXPRESS

tethered swallowable capsules that can be used in unsedated patients to image the entire esophagus [11, 75, 139] (Fig. 16). Different OCT tethered capsule endomicroscopy (TCE) devices have now been used in nearly 100 patients, showing that the procedure only takes about 5 minutes and is preferable over endoscopy for nearly 90% of patients [75, 140]. These initial findings suggest that OCT-based TCE may become an important new clinical screening tool for BE.

While EAC is the most common form of esophageal cancer in the US and Europe, squamous cell cancer (SCC) is more common in other areas of the world, notably China and Africa. The majority clinical studies have focused on the use of OCT for early (Tis/T1a/T1b) SCC staging [141–143], which is not adequately performed with standard of care endoscopic ultrasound (EUS) and is critical for patient management decisions. OCT criteria established for staging SCC showed good accuracy for differentiating cancer invasion in epithelium/lamina propria (94.9%), mascularis mucosa (85%) and submucosa (90.9%) [142]. In another study by the same group accuracy of OCT cancer staging was compared to that of high-frequency ultrasound [143]. The accuracy of OCT for distinguishing superficial SCC limited to epithelium/lamina propria was 95% and 85% for muscularis mucosa/submucosa invading lesions. The accuracy of high-frequency ultrasound was significantly lower with 80% accuracy for superficial and 70% for more invasive lesions [143].

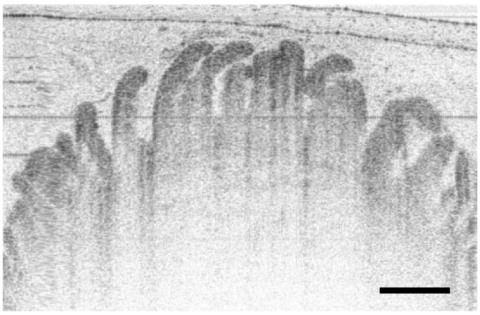

Fig. 17. Duodenal villi seen by OCT. Scar bar: 500 μm.

Stomach and small intestine: While still in early stages of investigation, OCT has been used in several clinical studies to image the stomach and first portion of the intestine (duodenum). The large size of the stomach is a challenge for existing OCT probes designs. However, preliminary results show promise for OCT to be capable of differentiating normal stomach [6, 33, 144, 145] from cancerous tissue [55] that has typically higher homogeneity, epithelial backscattering, and vascularization [55]. Most investigations in the duodenum utilized a helically scanning probe through the accessory port of an upper endoscope [6, 145]. Findings showed that the intestinal villi can be clearly visualized by OCT (Fig. 17), as well as microvascularity of villi using Doppler OCT [36]. These results are important, as blunting of these villi can be an indicator of celiac disease, which today still frequently requires a tissue diagnosis prior to initiating a gluten-free diet. Since the disease can be patchy, biopsies often come back negative even after positive serology. OCT, with its capability to image entire luminal organs, can change this equation by comprehensively imaging large regions of the duodenum to assess villous blunting without the sampling error that is inherent in endoscopic biopsy [146]. Indeed, a recent study showed that OCT has a sensitivity and specificity of 82% and 100% [147], respectively, compared to histology, adding further evidence for its potential to improve our capacity to obtain a tissue diagnosis of celiac disease.

Large intestine (colon), Another important potential application of OCT in the GI tract is the identification and diagnosis of colon polyps. Currently, endoscopically-identified polyps are taken out of the colon and examined by histopathology to determine if they are pre-malignant (adenomas) or benign (hyperplastic polyps). While this scheme has served patients

Biomedical Optics EXPRESS

well for the past 50 years, there are circumstances where this strategy falls short. In some patients who have many polyps, for example those with familial polyposis syndromes or with ulcerative colitis, it is impractical to take all polyps out of the patient. In addition, some lesions, most commonly sessile serrated adenomas, are not easily identified by endoscopy and are therefore often missed. For these reasons, there is a rationale to consider using an *in vivo* microscopy technology like OCT to attempt to identify and diagnose lesions in the colon.

To date, there have been a few *in vivo* studies using OCT for differentiating benign form neoplastic polyps. Following a few preliminary reports using OCT to show the normal microscopic architecture of the human colon [5, 6, 148], three studies demonstrated a significant decrease in light scattering and a higher degree of disorganization in adenomas in patients with colorectal cancer in comparison to hyperplastic polyps (Fig. 18) and nonpolypoid normal tissue [21, 145, 149]. A larger number of patients have been enrolled to determine the potential of OCT for diagnosing and differentiating inflammatory bowel disease (IBD). The first IBD study was published in 2004, showing a sensitivity of 90% and specificity of 83.3% for distinguishing Crohn's disease from ulcerative colitis using OCT-based detection of transmural inflammation [150]. A subsequently published detailed analysis of OCT features of ulcerative colitis demonstrated similar results [151]. In all of these studies, OCT analyses were performed based on two-dimensional OCT images. Three-dimensional reconstruction of the ulcerative colitis section was presented by Adler et al. showing *en face* image that emphasized presence of large subsurface voids and ulcerations, and absence of regular crypt pattern [152].

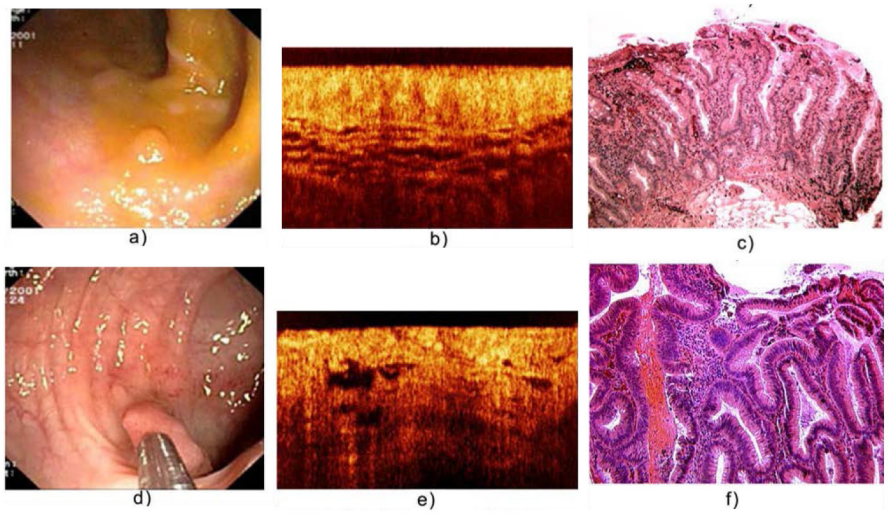

Fig. 18. Endoscopic, OCT and the corresponding histologic images of hyperplastic polyp (a-c); adenomatous polyp (d–f). (Figure and caption adapted from [21].)

Biliary/pancreatic tract: The main application for microscopic imaging of the bile duct is to identify the nature of bile duct strictures, which may be primary cancer (cholangiocarcinoma), metastatic cancer, primary sclerosing cholangitis, primary biliary cirrhosis, or other inflammation caused by the like of biliary stones. Current methods of investigation, including endoscopic retrograde cholangiopancreatography (ERCP) or biliary endoscopy with brush biopsy [153] are inadequate as often the pathology resides below the surface and cannot be seen by these techniques.

Biomedical Optics EXPRESS

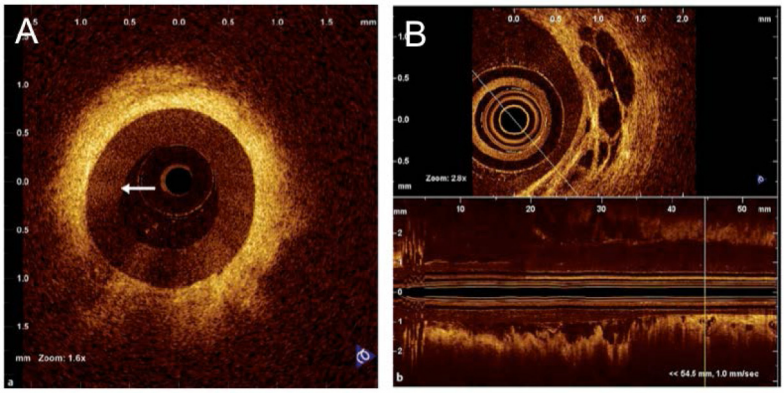

Fig. 19. (A) Radial OCT image of the common bile duct in a patient with a benign stricture following cholecystectomy. The probe is surrounded by the endoscopic retrograde cholangiopancreatography catheter (arrow). (B) OCT criteria - large, non-reflective areas contained in the intermediate layer - suggesting tumor vessels. Both axial section and longitudinal reconstruction are depicted. (Figure and caption adapted from [154], by permission from Macmillan Publishers Ltd.)

Rotational and helical scanning OCT probes have been utilized in small studies in the bile duct system. Predominantly pilot clinical studies have been conducted with OCT [154–157]; this early data suggests that different types of strictures do indeed have distinct microscopic morphologic features (Fig. 19). With the recent introduction of commercial systems to image the bile duct, it is quite possible that OCT may become a valuable adjunct technology to ERCP for distinguishing the nature of indeterminate biliary strictures.

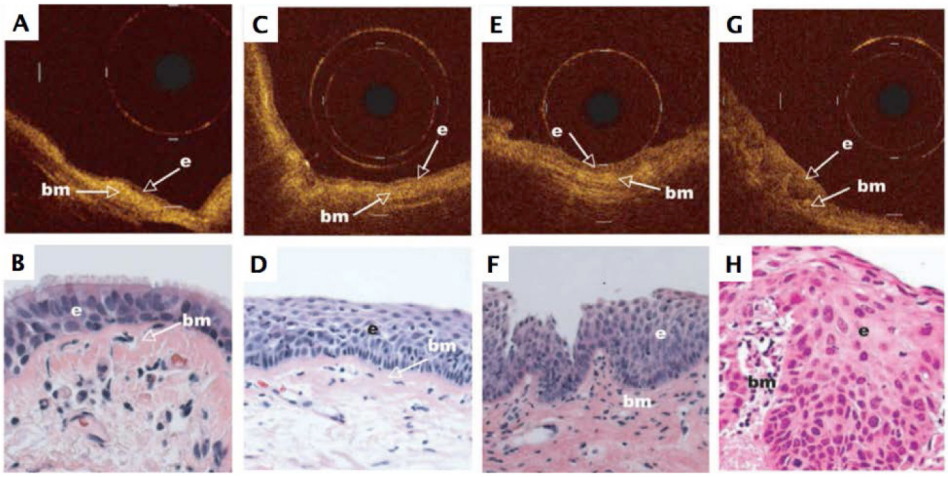

Fig. 20. Representative OCT images (top row) and corresponding standard histologic section (H&E stain; original magnification, x20, bottom row) of: (A, B) normal healthy human bronchus showing a single-layer epithelium (e) on top of the basement membrane (bm) and upper submucosa; (C, D) an area with metaplasia; (E, F) an area with moderate dysplasia; and (G, H) an area with carcinoma in situ. Each calibration mark in the OCT image is equal to 1mm. (Figure and caption adapted from [158], with permission from AACR.)

3.3 Pulmonary tract

Lung cancer: Lung cancer is the most common cause of cancer-related death [159]. New methods capable or diagnosing of lung cancer early and correctly characterizing the specific type of cancer are necessary to improve screening and to optimize treatment planning. Many

Biomedical Optics EXPRESS

studies have centered on the use of OCT in lung cancer both as an *in vivo* diagnostic tool and to guide biopsy acquisition in order to increase diagnostic yield [158, 160, 161]. One of the first clinical studies in 2005 utilized helically scanning OCT catheter introduced into the bronchial lumen of cancer patients under anesthesia via working channel of a bronchoscope [160]. OCT results showed that neoplasia could be characterized by unevenly distributed, high back scattering regions and loss of the homogenous appearance of normal mucosal and submucosal layer [160]. Following this early feasibility study, pre-neoplastic changes found by autofluorescence bronchoscopy in the bronchial epithelium of 138 heavy smokers participating in a chemoprevention trial and 10 patients with lung cancer were imaged using OCT (Fig. 20). The results showed that OCT was capable of differentiating dysplasia and carcinoma in situ from normal tissue, hyperplasia, or metaplasia based on a progressive increase in the epithelial thickness and surface maturation, however, it was not possible to differentiate between high-grade dysplasia and carcinoma in situ [158].

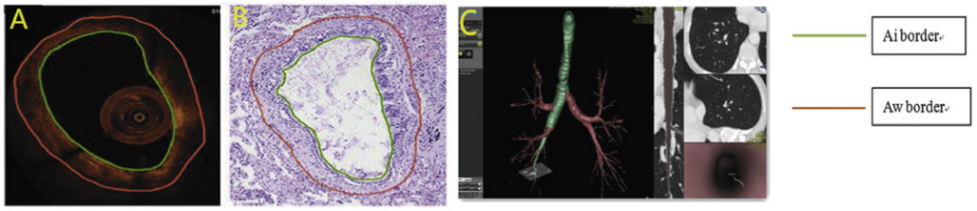

Fig. 21. Endobronchial OCT, histology and CT measurement matching. (A) OCT measurement vision; (B) Histology measurement vision; (C) CT measurement vision. (Figure and caption adapted from [162], with permission from Elsevier.)

Airway remodeling: Airway remodeling is a crucial feature for the early detection and prognostic assessment of diseases such as chronic obstructive pulmonary disease (COPD) and asthma. OCT changes in airway architecture in patients with more advanced COPD can be detected before functional abnormalities [163]. Comparison of OCT measurements of airway dimensions, like lumen and wall area in patients with obstructive airway disease showed a strong correlation to results from computed tomography, which is currently used for assessment of airway remodeling in addition to pathological analysis of surgical specimens [164]. A strong correlation in lumen and wall thickness diameters between OCT and CT images in COPD patients and patients with pulmonary nodules was also found in peripheral airways [162] (Fig. 21). In another study, the reproducibility of OCT measurements was evaluated by inserting and then reinserting the OCT probe in the airways of current or former smokers [165]. Inter-observer variability of 12% was obtained for wall thickness measurements and 9% for intra-observer analysis [165]. OCT was also used to investigate tissue remodeling prior to and 2 years after bronchial thermoplasty in 2 asthma patients, where reduction in airway thickness was compared for treated and untreated patients [166].

Biomedical Optics EXPRESS

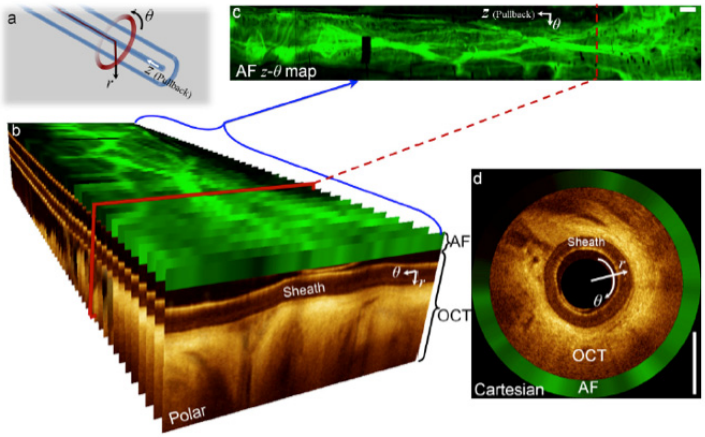

Fig. 22. OCT-AFI image presentation: (a) coordinate system defined with respect to the catheter tip, (b) OCT-AFI frames along the pullback presented in polar coordinates, *en face* AFI z-θ image, and (d) an OCT-AFI frame presented in Cartesian coordinates. Scale-bars are 1mm. (Figure and caption adapted from [167].)

Microvasculature, autofluorescence and birefringence: To further increase clinical utility of OCT in pulmonary medicine, multi-modal endobronchial OCT imaging techniques to enhance contrast and improve visualization of microstructure/function were introduced [167, 168]. For example, visualization of the 3D vascular network in the lung has the potential to improve detection and monitoring of diseases like asthma, chronic obstructive pulmonary disease and cancer. The results from a novel intraframe data processing method to extract Doppler information enabled visualization of small (~80 μm) and large (~1mm) vessels in patients, with better frame-to-frame stability and relative insensitivity to subject and/or probe motion [169]. To provide additional insight into the complex vasculature and tissue microstructural remodeling associated with pulmonary pathology, including lung cancer, a multi-modal Doppler OCT and autofluorescence bronchoscopy imaging system was developed by Pahlevaninezhad et al. [167, 170] (Fig. 22). The multi-modal system provided rapid identification of pulmonary nodules while also highlighting major vessels for biopsy guidance [167], and visualizing vessels as small as 12 μm [170].

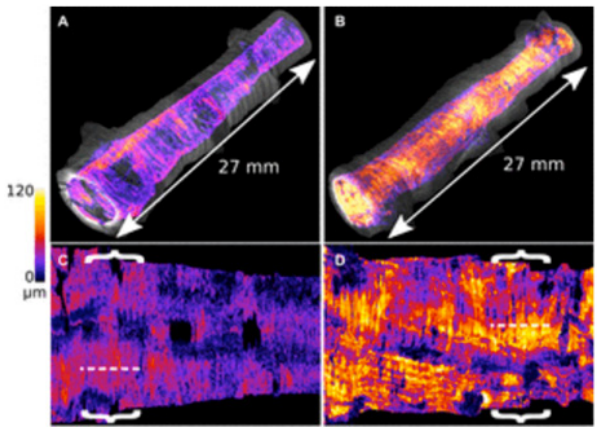

Fig. 23. Morphological comparison between asthmatic and healthy control human subjects *in vivo* with OR-OCT. Circularized volumetric image from a 2.7-cm endoscopic pullback of a (A) healthy control and an (B) allergic asthmatic subject acquired from similar regions in the right upper lobe. (C and D) Unwrapped and two-dimensional representations of the airway segments depicted in (A) and (B). Dashed lines and brackets, 6 mm. (Figure and caption adapted from [168]. Reprinted with permission from AAAS.)

Biomedical Optics EXPRESS

Another example of a contrast-enhancing technique is orientation resolved OCT (OR-OCT) that is based on polarization sensitive OCT [168]. This technology, utilizes the optical axis of tissue birefringence to highlight ordered structures within the tissue such as airway smooth muscle. Such contrast can be an important biomarker in the assessment of asthma (Fig. 23) [168] and in other obstructive lung diseases such as COPD [168].

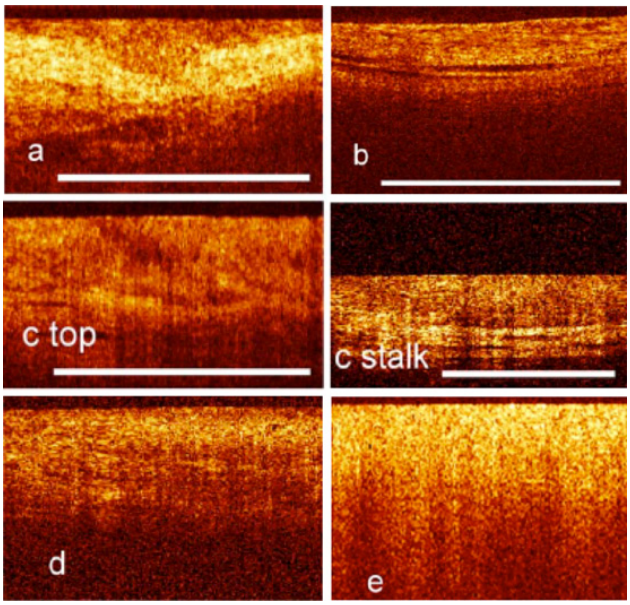

Fig. 24. Pathologic findings on optical coherence tomography imaging of the bladder: (a) dysplasia; (b) carcinoma in situ; (c) papillary Ta lesion; (d) T1 lesion; (e) muscle-invasive urothelial cell carcinoma. (Figure and caption adapted from [171], with permission from Elsevier.)

3.4 Urinary tract

Bladder: OCT has a potential role in following lesions in the bladder that are suspicious for bladder cancer. For *in vivo* imaging of the urinary tract, front-viewing OCT catheters are introduced via working channel of the cytoscope. With early systems, it has been shown that OCT has 100% sensitivity and 89% specificity for diagnosing transitional cell carcinoma based on differentiating its OCT appearance from inflammation and dysplasia [172]. Introduction of MEMS-based micro scanning mechanisms enabled further improvement of OCT probes, resulting in 4.5mm long scans at 8fps allowing for combining cross-sectional information with information about mucosal blood flow [173]. Using commercially available laparoscopic system, OCT was shown to be capable of staging tumors, including identifying muscle-invasive bladder tumors [174], reducing false-positive findings of fluorescence cystoscopy (Fig. 24) [171]. Combination of fluorescence cystoscopy with cross-polarization OCT, which provides quantitative information about microsctructural changes in collagen, demonstrated an accuracy, sensitivity and specificity above 90% for detecting flat suspicious lesions [175]. The cross-polarization OCT system was also used to detect tissue fibrosis caused by chronic inflammation or post-radiation reaction [176].

Biomedical Optics EXPRESS

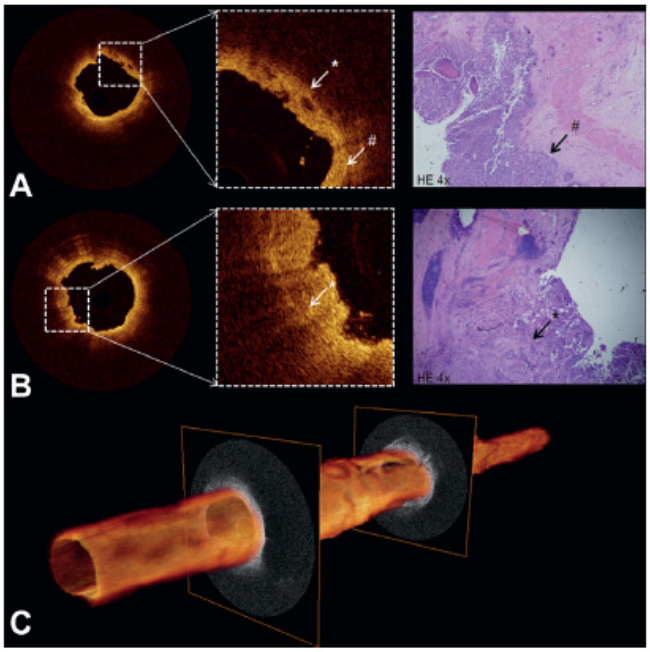

Fig. 25. (A) and (B) cross-sectional OCT images of proximal ureter show interruption (white asterisk) of thin dark line (white pound sign), suggesting invasive tumor. Corresponding histology revealed T3G3 urothelial carcinoma (black arrow). (C) 3D pullback of OCT built from 520 individual cross-sectional images over 5.2 cm length. (Figure and caption adapted from [177], with permission from Elsevier.)

Ureters: The luminal nature of ureters allows for volumetric OCT imaging with cardiovascular catheters. In a pilot clinical study, Bus et al. investigated the use of endoscopic OCT in patients with suspicion or undergoing follow up of urothelial carcinoma [177]. Cardiovascular catheters were introduced into the upper urinary tract using ureterorenoscope and healthy and cancerous tissues were imaged (Fig. 25). In a larger study, the sensitivity and specificity of OCT for staging urethral tumors was 86.7% and 78.6% respectively and for grading, 91.7% and 78.6%, respectively [178].

Prostate: The management of prostate cancer, which is the second most common cause of cancer-related death in men in the US, may be enhanced by the utilization of OCT. Prostate cancer treatment requires radical prostectomy during which it is crucial to preserve small vessels and nerves to avoid incontinence and sexual dysfunction complications. In one study, a reusable 2.7 mm front-viewing probe was inserted through laparoscopic port during prostate resection to differentiate neurovascular bundles from nerve tissue, prostate capsule, fat, and lymphatics. These early results showed the potential of laparoscopic OCT to be a useful tool during nerve-sparing surgical procedures [179].

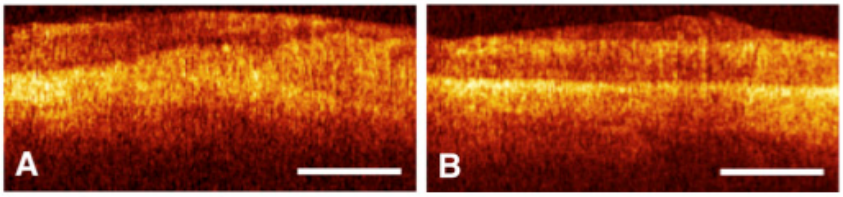

Fig. 26. OCT tomograms of the cervix after electrosurgery: (A) two weeks later (zone of necrosis - right); (B) six weeks after (normal epithelium seen as an even stripe). Scale bars, 500 μm. (Figure and caption adapted from [180].)

Biomedical Optics EXPRESS

3.5 Gynecologic tract

Cervix and uterus: Cervical cancer is the fourth most common cause of cancer related death in women [159]. Cervical cytology with a Pap smear test is a current standard of care for cervical cancer screening. If cancer is diagnosed at an early stage, a minimally invasive treatment aimed at organ and function preservation is possible. In such cases, it is important to correctly delineate the margins of the disease. Preliminary results, obtained with a front viewing line scan endoscopic OCT probe, demonstrated that OCT was capable of differentiating cervical cancer at various stages [55, 180]. OCT has been also used to monitor the effectiveness of early stage cancer treatment with electroexcision and laser vaporization. OCT imaging was performed immediately after the procedure, as well as up to few weeks after to monitor changes of the zone of necrosis (Fig. 26) [180]. Changes in architecture of the squamous epithelium of cervix were also investigated as a function of hormonal changes caused by age or pregnancy [180]. The same OCT probe design was also used during standard hysteroscopy to image the uterine cavity in patients with tumor-like processes in endo- and myometrium [55]. Preliminary results showed that endometrial microarchitecture (e.g. thickness, endometrial glands) changed in concert with age and menstrual cycle [55]. OCT was also capable of providing differential diagnosis between submucosal myoma and glandular fibrous polyps [55].

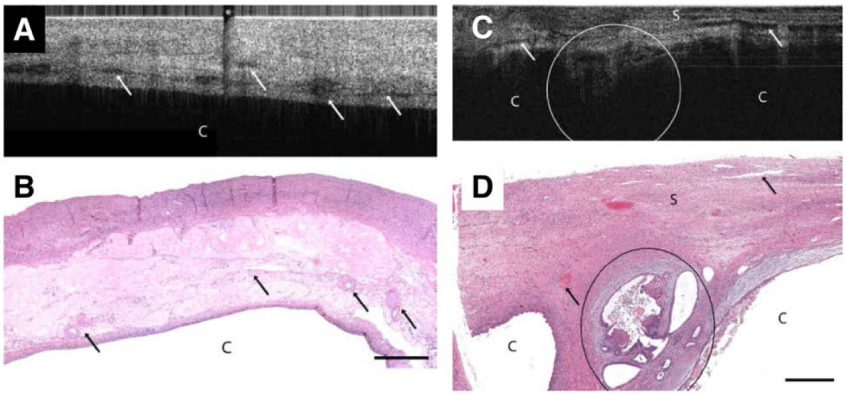

Fig. 27. (A) OCT image of papillary serous cystadenoma (4x1.4 mm) and (B) corresponding histopathology. (C) OCT image of endometrioid adenocarcinoma (4x1.4 mm) and (D) corresponding histopathology. OCT and histopathology images are to scale. Scale bar, 500 µm. C: cyst, Arrows: blood vessels, S: stroma, circled region: malignant glands, asterisk: imaging system artifact. (Figure and caption adapted from [181], with permission from Elsevier.)

Ovaries and fallopian tubes: Ovaries can potentially be accessed from the uterus via the very thin fallopian tubes. Even though small OCT catheters, such as those used for cardiovascular imaging, could be compatible with the diameter of fallopian tubes, navigating the catheter through tortuous segments of the tubes is challenging. Thus, most OCT studies of the ovaries have been performed through minimally invasive laparoscopic procedures with specially designed rigid laparoscopic OCT probes. Laparoscopy is a common treatment procedure in patients with ovarian cancer. Due to the lack of specific symptoms, ovarian cancer is commonly diagnosed at advanced stage, often after it has metastasized. It is paramount to correctly differentiate tumor from normal tissue to resect the entire tumor. The laparoscopic OCT probe was used in peri- or post-menopausal women undergoing laparoscopic oophorectomies [181]. OCT results obtained *in vivo* were correlated with histology of excised specimens, demonstrating that OCT is capable of differentiating normal ovarian tissue from endometriosis, cystadenoma, and adenocarcinoma [181] (Fig. 27).

Assessment of proper functioning of fallopian tubes is crucial to understand causes of female infertility. Morphological changes often caused by inflammation can impair proper

Biomedical Optics EXPRESS

functioning of this part of the reproductive system. If no significant imperfections of fallopian tubes are observed during transvaginal ultrasound examination, CT scan, MRI or hysterosalpingogram, laparoscopic examination is often performed to diagnose pelvic inflammatory disease (PID). Laparoscopic examination has only 27% sensitivity and 92% specificity [182] for diagnosing inflammatory disease - an additional tool to improve sensitivity is necessary for optimal management of patients. In one study with a laparoscopic OCT probe, patients with and without PID were imaged. OCT criteria developed based on analysis of OCT-histology correlated images were validated, showing 90% sensitivity and 81% specificity for the diagnosis of inflammatory changes in fallopian tubes [183].

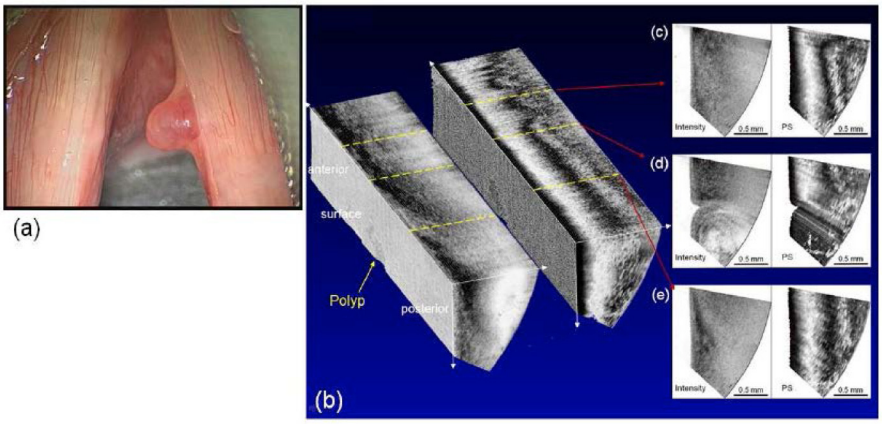

Fig. 28. Wide field image (a), 3D PS-OCT image of polyp (b, intensity: left, PS: right), and cross-sectional images (c-e). (Figure and caption adapted from [23].)

3.6 Otolaryngology

Larynx: The main application of OCT in the field of otolaryngology is focused on imaging microstructures of various laryngeal pathologies, which can be of use for monitoring disease progression as well as for guiding biopsies and treatment [184]. Imaging could be performed during surgical endoscopy by directing the probe to the larynx through a laryngoscope [35, 185]. Such a forward scanning probe was used to establish a quantitative comparison between *in vivo* OCT measurements of epithelial thickness and light microscopy measurements on excised specimens [186]. To address a need for early cancer detection, a rigid OCT probe was developed that could be attached to the laryngoscope for office-based examination of patients without need of anesthesia [187]. The main challenge for the device was a limited field of view and short working distance of the OCT probe in comparison to the laryngoscope that caused difficulties in correct placement of the device. The next generation office-based device with much higher frame rates (40 fps) was also used for OCT examination of vibration frequency and magnitude of vocal cords [188]. In another approach, a flexible OCT probe was introduced through the nose to the larynx under endoscopic visualization in awake patients. To further improve results, a flexible OCT probe capable of polarization sensitive imaging sensitive to collagen distribution showed promise for assessing various epithelial changes, like keratosis, dysplasia, papillomas and cancer [189] and scar tissues [190]. In a later study with a next generation flexible probe that had MEMS scanner, enclosed in 2.7mm in diameter and 12mm in length rigid tip, large three-dimensional PS-OCT data sets were obtained, enabling the investigation of the spatial distribution of lesions [23] (Fig. 28). In recent study by Garcia et. al, a method based on analysis of attenuation coefficients in OCT data obtained in pediatric population was introduced to provide quantitative measure of vocal folds changes as a function of age [191].

Biomedical Optics EXPRESS

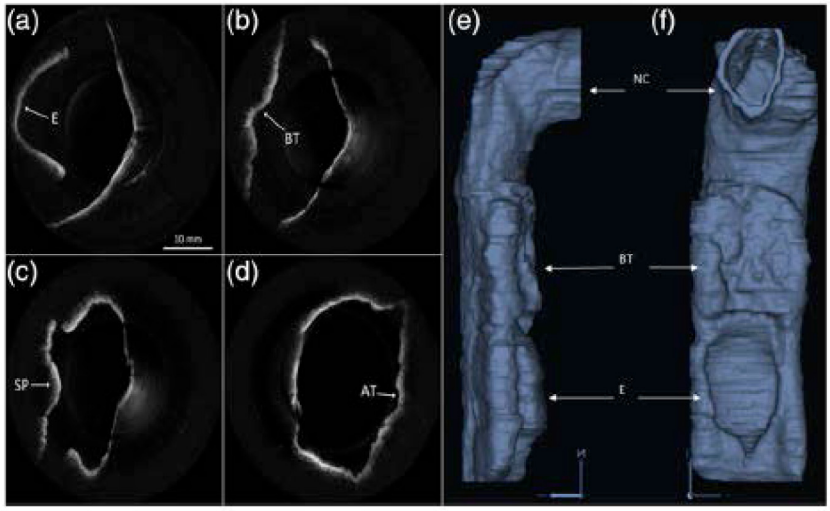

Fig. 29. *In vivo* OCT images of human upper airway covering hypopharynx (a), oropharynx (b) and (c), and nasopharynx (d). 3-D rendering profile view (e) and front-on view (f) from *in vivo* data. Epiglottis (E), base of tongue (BT), soft palate (SP), adenoidal tissue (AT), right nasal cavity (NC) are labeled. (Figure and caption adapted from [192].)

Global anatomy of the airway: In addition to morphological information about wall architecture, OCT can also provide information about the shape and size of the airway that can be used for better understanding the pathophysiology behind conditions like obstructive sleep apnea (OSA). In order to use OCT for imaging the global anatomy of the upper airways, its imaging range (commonly limited to less than 5mm) had to be significantly extend [193]. The longer imaging range of such endoscopic OCT systems, often called anatomic OCT (aOCT), came at the cost of a lower transverse resolution due to the need to extend the catheters' working distance and depth of focus. This technology was used in an overnight study, showing changes in upper airway caliber before, during, and after airway collapse in a patient with OSA [194]. Another anatomic SS-OCT system, capable of high-speed imaging (25 frames per second), was used to create three-dimensional reconstructions (Fig. 29) of airways with diameters up to 30 mm in unsedated patients [192]. The same system was also used to detect of injuries introduced by smoke inhalation [195]. The capacity of long-range OCT for simultaneous imaging of microanatomy and volumetric global anatomy reconstruction was also explored in evaluation of subglottic tissue in intubated neonatal airways (46 cases) [196].

Biomedical Optics EXPRESS

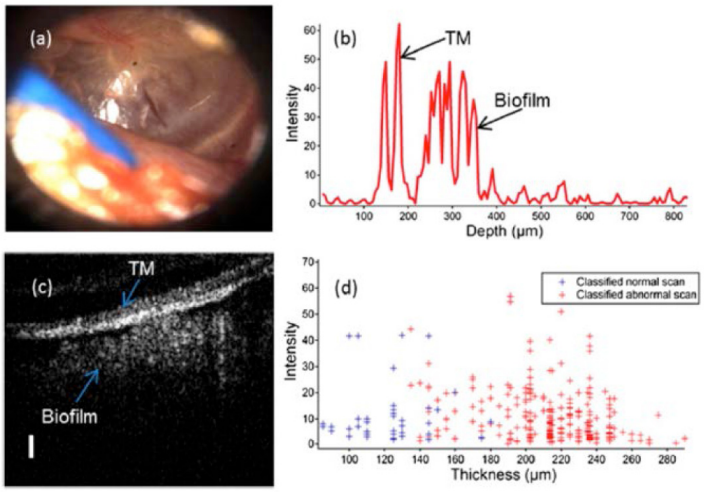

Fig. 30. Chronic middle-ear infection with a thick, highly scattering biofilm. (A) Video otoscopy image showing a less-translucent tympanic membrane (TM). (B) Typical OCT depth scan showing evidence of a thick (~200 μm average thickness) biofilm behind the TM. (C) Cross-sectional OCT image showing the lateral spatial extent of biofilm. (D) Classification results of the OCT scans demonstrating that 87% of acquired OCT scans were classified as abnormal. (Scale bar in C: 100 μm.) (Figure and caption adapted from [197].)

Ear: Another prominent application of OCT in otolaryngology is imaging of the human ear, especially focused on diagnosing chronic otitis media. This middle ear infection is common in the pediatric population and is often linked to the presence of a biofilm just behind the tympanic membrane. After the first clinical study showing tympanic membrane images in normal subjects and patients with various hearing problems [198], a number of studies focused on detection of biofilms [197, 199] (Fig. 30) and characterization of tympanic membrane [200–203] have been performed. Recently, a large effort has been placed on the development of a point-of-care hand-held diagnostic instrument that can be easily used in any health care setting [204]. Very recently, a long-range, wide-field SSOCT device has been published for real-time imaging of the whole middle ear in 3D in combination with Doppler virography [205]. In addition to the investigation of real-time microscopic dynamics of the middle ear this system can be also used for post-operative tracking of middle-ear prosthetics [205].

Nasal cavity: Interest in the application of OCT for the nasal cavity involves the management of patients with nose congestion in rhinitis caused by viruses, bacteria or allergies. OCT images showing nasal mucosa microanatomy were obtained in awake patients or in patients under general anesthesia during surgical endoscopy [206, 207]. Results showed that OCT could also visualize changes in tissue morphology during decongestant therapy [206] and could differentiate different types of rhinitis [207]. Most recently, there has been an interest in the examination of nasal mucosal changes that can be potentially significant for the assessment of cystic fibrosis. Studies with OCT in the nose have shown that in comparison to normal subjects, the thickness of the nasal mucosal layer in patients with cystic fibrosis was increased due to chronic inflammation [42] (Fig. 31). OCT was also found to be sensitive to changes in response to antibiotic therapy [42].

Biomedical Optics EXPRESS

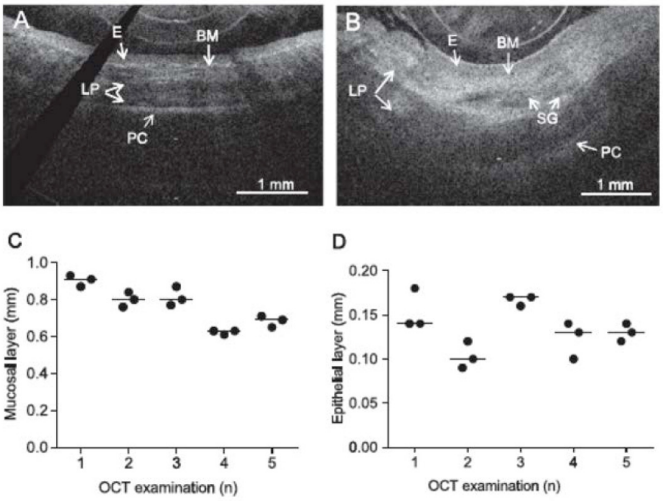

Fig. 31. OCT images of the nasal mucosa from a healthy control (A) and a patient with CF (B), showing the epithelium (E), basement membrane (BM), lamina propria (LP) with seromucinous glands (SG) and perichondrium (PC). Validation measurements of nasal mucosa (C) and epithelial layer thickness (D) by OCT imaging in healthy controls. Data are presented as individual data points and median. (Figure and caption adapted from [42], with permission from Elsevier.)

4. Summary

The field of endoscopic OCT has grown at an accelerating pace thanks to collaborative efforts between academia and industry, and among scientists, engineers, and clinicians. While we attempted to highlight different aspects of this field, given its large magnitude, it was not feasible to include all endoscopic OCT technologies and applications in this review.

With the recent FDA approvals of several endoscopic OCT technologies for cardiovascular and GI applications, endoscopic OCT technology is increasing in availability to clinicians and researchers. More clinical trials are expected in the upcoming years. Among many of the development fronts, the field has witnessed increasing interest in (1) exploring different spectral ranges to enhance imaging contrast and/or resolution, and (2) integrating OCT with other modalities, aiming to improve diagnostic sensitivity and specificity. As OCT finds broader applications, it is clear that standards are needed for uniform data collection and analysis to fully leverage the work being conducted in this area for assessing the clinical utility of this technology. Considering the large amount of image data that can be collected in real time, methods are also needed for handling large data sets, including new visualization and computer-aided enhancement techniques; such developments will help reveal the most critical diagnostic information in a timely manner.

Disclosures

Massachusetts General Hospital has licensing arrangements with Terumo Corporation, NinePoint Medical, and LX Medical. Dr. Tearney has the rights to receive royalties from licensing arrangements Terumo Corporation and NinePoint Medical. Dr. Gora has the rights to receive royalties from licensing arrangement with NinePoint Medical. Dr. Suter has the rights to receive royalties from licensing arrangements with NinePoint Medical and LX Medical. Dr. Tearney consults for NinePoint Medical. Dr. Suter consults for LX Medical. Dr. Tearney receives catheter materials from Terumo Corporation.

Johns Hopkins University has licensing arrangements with Microtech Ltd. Dr. Li has the rights to receive royalties from the licensing arrangements.

Biomedical Optics EXPRESS

Acknowledgments

The authors would like to thank Dr. Hyeon-Cheol Park (Department of Biomedical Engineering, Johns Hopkins University) for helping prepare some of the design schematics.